https://doi.org/10.5194/egusphere-2026-5525
Preprint. Discussion started: 23 September 2026

Quantifying future Arctic and Antarctic climate change from a storyline perspective using global variable-resolution models

Lise Seland Graff[1], Dörthe Handorf[2], Raphael Köhler[2], Xavier Levine[3,a], René R. Wijngaard[4], Ryan S. Williams[5], Gareth J. Marshall[5], and Priscilla A. Mooney[3]

[1]Norwegian Meteorological Institute, Oslo, Norway
[2]Alfred Wegener Institute, Helmholtz Centre for Polar and Marine Research, Potsdam, Germany
[3]NORCE Norwegian Research Centre AS and Bjerknes Centre for Climate Research, Bergen, Norway
[a]now at: Department of Earth and Environmental Sciences, Columbia University, New York, USA
[4]Utrecht University, Utrecht, the Netherlands
[5]British Antarctic Survey, Cambridge, UK

Correspondence: Lise Seland Graff (lise.s.graff@met.no)

Abstract. Future climate projections are subject to multiple sources of uncertainty. Here, we examine model uncertainty from a storyline perspective using three variable-resolution (VR) models: the Community Earth System Model, the Icosahedral Nonhydrostatic model, and the Model for Prediction Across Scales. We implement the storyline framework by prescribing sea surface temperatures (SSTs) and sea-ice concentrations (SICs) from models from the coupled model intercomparison project phase six previously deemed representative of contrasting Arctic and Antarctic storylines. We perform experiments with and without polar refinement, resulting in the first storyline-based multi-model experiments with polar refinement.

We evaluate whether this framework captures known characteristics of the storylines and generally find good agreement between the VR experiments and storylines for near-surface temperature, reflecting the strong constraint from the lower-boundary forcing. For precipitation and zonal wind, the characteristics are better captured for the Antarctic storyline experiments than the Arctic ones. Nevertheless, the contrasting storyline forcing mostly yields distinct future responses, demonstrating that storyline-based forcing-model selection is a powerful tool for generating contrasting model experiments.

We also quantify the influence of the storyline, VR model, and resolution for a wider range of variables. Resolution has the weakest overall impact, while the storyline dominates across most variables in the Antarctic storyline experiments and for low-level tropospheric temperature and near-surface humidity in the Arctic experiments. The model and resolution influence are generally strongest for precipitation and cloud cover. Thus, the choice of lower-boundary forcing and model has a greater influence on future responses than local changes in horizontal resolution.

1 Introduction

Future climate projections, such as those developed under the Coupled Model Intercomparison Project (CMIP), are important resources for understanding the evolution of the global climate system, assessing the impacts of climate change, and developing adaptation and mitigation policies (e.g., van Vuuren et al., 2011; O'Neill et al., 2016; van Vuuren et al., 2025). However, these multi-model projections are also characterized by uncertainty, arising from internal variability, scenario uncertainty, and model uncertainty, that is, models responding differently to the same forcing (Hawkins and Sutton, 2009). The uncertainty of projected future warming is particularly large in the polar regions, as shown by Taylor et al. (2022) for the sixth phase of CMIP (CMIP6).

One source of model uncertainty is processes that cannot be explicitly resolved at the relatively coarse spatial resolution typically used by CMIP6 models. While employing high resolution globally can be challenging due to the high computational cost, global variable-resolution (VR) models allows for using high horizontal resolution in one or multiple regions of particular interest and coarser resolution elsewhere. Such models have been used to explore a wide range of topics including the influence of refinement on future extremes (e.g., Loeb et al., 2024; Wijngaard et al., 2025), model biases (e.g., Gettelman et al., 2018; Herrington et al., 2022; Wijngaard et al., 2023; Graff et al., 2026a), the response to idealized sea surface temperature (SST) changes (Wills et al., 2024), and the response to Arctic sea-ice loss (Sun et al., 2026).

Here, we take a combined VR-model and storyline approach to examine model uncertainty. We define storylines as physically plausible potential future scenarios, following Zappa and Shepherd (2017). We employ two Arctic and two Antarctic storylines of future climate change from Levine et al. (2024) and Williams et al. (2024) (hereafter L24 and W24), respectively. The storylines were derived from the CMIP6 multi-model ensemble for the extended summer seasons, May–October (MJJASO) for the Arctic and December–March (DJFM) for the Antarctic, and represent contrasting future changes based on storyline predictors that explain a large fraction of the total variance of key climate variables.

In L24, the predictors are Arctic amplification (AA) and Barents-Kara-Sea warming, and the most contrasting storylines represent: **weak** AA and **strong** warming in the Barents-Kara Seas (*storyline Arc-1*) and **strong** AA and **weak** warming in the Barents-Kara Seas (*storyline Arc-2*). In W24, the predictors are the loss of Southern Hemisphere (SH) sea-ice extent (hereafter sea-ice loss) and the anthropogenic-forcing-induced delay in the stratospheric polar vortex (SPV) summer breakdown (hereafter SPV breakdown; Mindlin et al., 2020); the most contrasting storylines are: **high** sea-ice loss and **early** SPV breakdown (*storyline Ant-1*) and **low** sea-ice loss and **late** SPV breakdown (*storyline Ant-2*).

We examine these four storylines using three VR models, the Community Earth System Model (CESM; Danabasoglu et al., 2020), the ICOsahedral Nonhydrostatic model (ICON; Zängl et al., 2015), and the Model for Prediction Across Scales (MPAS; Skamarock et al., 2012), combined with daily SST and sea-ice concentrations (SICs) from models from the CMIP6 ensemble that were found by Graff et al. (2026b) and W24 to be representative of the storylines (*the storyline models*). The representativeness of the storyline models was based on their proximity to the storylines in predictor space and historical performance.

Our storyline experiments are "AMIP-style", that is, similar to the Atmosphere Model Intercomparison Project (AMIP) experiments (e.g., Eyring et al., 2016), with active atmosphere and land components and simplified ocean and sea-ice models that employ SSTs and SICs from forcing files. For each storyline, we performed CESM, ICON, and MPAS experiments for the future (2090–2099) with polar refinement and uniform coarser resolution (*refined* and *unrefined* experiments), and unrefined experiments for the recent past (2005–2014). The SSTs and SICs were taken from the respective storyline model's Shared Socioeconomic Pathway corresponding to a 8.5 W m^{-1} increase in radiative forcing by the end of the 21st Century experiment (SSP5-8.5; O'Neill et al., 2016) and CMIP6 historical experiments (Eyring et al., 2016). To the best of our knowledge, the result is the first storyline-based multi-model experiment set with polar refinement. The experiments are complimentary to those in Graff et al. (2026a), as we employ the same models, grids, and conceptually-aligned experimental design.

https://doi.org/10.5194/egusphere-2026-5525
Preprint. Discussion started: 23 September 2026

The purpose of this study is threefold: (1) to document the VR-model storyline experiments and their common protocol; (2) to assess the extent to which storyline-based selection of contrasting SST and SIC fields yields distinct future responses and whether these responses capture the known storyline characteristics documented by L24 and W24; and (3) to assess and quantify the influence of the storyline forcing, the VR model, and the resolution on future responses. To address the second objective, we examine three target variables from L24 and W24: near-surface temperature, 850-hPa zonal wind, and total precipitation rate, highlighting the seasons the storylines were designed for (MJJASO and DJFM). For the third objective, we develop novel metrics based on pattern correlation coefficients for the future responses, considering a wider range of variables.

In what follows, we summarize the documented characteristics of the Arctic and Antarctic storylines from L24 and W24 in section 2, describe the new VR-model storyline experiments, their common experimental protocol, and the participating VR models in section 3, and we introduce the metrics that quantify the storyline, VR-model, and resolution influence in section 4. We then present results from the Arctic and Antarctic storyline experiments in section 5 and 6, respectively, before summarizing and discussing our findings in section 7. Additional tables and figures are available in the supplementary material.

2 Previously derived storylines and storyline models

Data from large multi-model ensembles have traditionally been analyzed by considering changes in the multi-model mean. The storylines approach (Zappa and Shepherd, 2017) offers a way of exploring the substantial diversity found in the simulated response to future warming, by synthesizing plausible scenarios of climate change dependent on the response of the atmospheric circulation which dominates uncertainty in the extratropics (Deser et al., 2012b; Shepherd, 2014). Storylines of future climate change are identified by conditioning regional changes or impacts upon the existence of plausible future changes (drivers), such as those related to the atmospheric circulation or specific warming patterns.

Recently, storylines optimized for the Arctic and Antarctic were derived by L24 and W24, respectively, using data from the historical and SSP5-8.5 experiments from the CMIP6 multi-model ensemble. Both studies applied a multiple linear regression framework in which selected drivers are represented by regression terms scaled by the global-mean near-surface temperature change between SSP5-8.5 and the historical experiment. This scaling separates uncertainty associated with atmospheric circulation response from that associated with global warming, following the pattern-scaling assumption (Tebaldi and Arblaster, 2014).

L24 derived Arctic storylines for the extended boreal summer season (MJJASO) using the strength of AA and the strength of the sea-surface warming over the Barents-Kara Seas as drivers. While L24 considered four storylines, we selected the two that maximize the drivers' diversity (Table 1): *weak* AA combined with *strong* SST warming in the Barents-Kara Seas (Arc-1 here and A in L24) and *strong* AA combined with *weak* SST warming in the Barents-Kara Seas (Arc-2 here and D in L24).

Compared to the CMIP6 multi-model mean, Arc-1 is characterized by a relatively warm marine Arctic, Arctic-adjacent continents that are comparatively cool and humid, and a weaker poleward shift in the North-Atlantic jet. Conversely, Arc-2 is characterized by a relatively cool marine Arctic, warm and dry high-latitude continents, and a stronger poleward shift in the North Atlantic jet.

https://doi.org/10.5194/egusphere-2026-5525
Preprint. Discussion started: 23 September 2026

Table 1. Overview of Arctic and Antarctic storylines. For each storyline (column 1), we provide the two predictors (column 2—3), the season (column 4), the storyline model and its short name (column 5–6), and the realization used for the storyline model's CMIP6 historical and SSP5-8.5 experiments (column 7). We use WACCM as a short name for CESM2-WACCM to distinguish it from the VR version of CESM2.

Storyline	**Storyline predictors**		**Season**	**CMIP6 model**	**Short name**	**Realization**
Ant-1	*High* sea-ice loss	*Early* vortex breakdown	DJFM	CESM2-WACCM	WACCM	r1i1p1f1
Ant-2	*Low* sea-ice loss	*Late* vortex breakdown	DJFM	MPI-ESM1-2-LR	MPI	r1i1p1f1
Arc-1	*Weak* AA	*Strong* Barents-Kara Sea warming	MJJASO	CNRM-ESM2-1	CNRM	r1i1p1f2
Arc-2	*Strong* AA	*Weak* Barents-Kara Sea warming	MJJASO	NorESM2-MM	NorESM	r1i1p1f1

W24 derived four Antarctic storylines for the extended austral summer season (DJFM) based on sea-ice loss and the delay in the summertime breakdown of the SPV. While their study also includes storylines for winter, we only consider the summer storylines here for consistency with the Arctic and because the explained variance is higher. As for the Arctic, we select the two storylines with the most contrasting climate responses (Table 1): *high* sea-ice loss combined with *early* vortex breakdown (Ant-1 here and B in W24) and *low* sea-ice loss combined with *late* vortex breakdown (Ant-2 here and C in W24).

Both drivers strongly influence the eddy-driven jet, which in turn modulates near-surface temperature and precipitation across the Antarctic. However, the SPV term is more than twice as influential as the sea-ice-loss term (W24, their Fig. 3). For Ant-2, both the poleward shift and strengthening of the jet is about twice that of storyline Ant-1 (W24, their Fig. 6 and Table 3), with the warming over the Antarctic continent and surrounding seas reduced by about 50%. Precipitation is more consistent for both storylines, with an increase around Antarctica that is likely dominated by the thermodynamic effect which prevails at high-latitudes, but is slightly enhanced for Ant-2 relative to Ant-1. This is likely to have significant ramifications for surface mass balance along coastal regions of Antarctica, integrity of ice shelves and resultant sea level rise (Scambos et al., 2013; Banwell et al., 2019; Lai et al., 2020; Gilbert and Kittel, 2021; Gilbert et al., 2025).

Graff et al. (2026b) and W24 identified storyline models from CMIP6 based on their proximity to the Arctic and Antarctic storylines in predictor space and their historical performance. We use the models they selected for Arc-2, Ant-1, and Ant-2: the second version of the Norwegian Earth System Model at medium resolution (NorESM2-MM; Seland et al., 2020), the CESM2 configured with the Whole Atmosphere Community Climate Model (CESM2-WACCM; Gettelman et al., 2019; Danabasoglu et al., 2020), and the Max Planck Institute Earth System Model version 1.2 at low resolution (MPI-ESM1-2-LR; Mauritsen et al., 2019). For Arc-1, we use the second version of the CNRM-CERFACS Earth System Model (CNRM-ESM2-1; Séférian et al., 2019) to optimize comparability with simulations from the polar coordinated regional downscaling experiment (Polar CORDEX) and PolarRES (Gilbert et al., 2026; Köhler et al., in prep.; Mooney et al., in prep; Mottram et al., 2026). For brevity, we hereafter refer to the storyline models as CNRM, NorESM, WACCM, and MPI (Table 1).

https://doi.org/10.5194/egusphere-2026-5525
Preprint. Discussion started: 23 September 2026

Table 2. Overview of the recent-past (2005–2014) and future (2090–2099) VR-model experiments. For each set of SST and SIC forcing fields (column 1), we list the unrefined (unref) and refined (ref) experiments carried out with CESM, ICON, and MPAS (column 2–4).

SST & SIC	CESM runs	ICON runs	MPAS runs
CNRM historical	Arc-1 recent-past unref	Arc-1 recent-past unref	Arc-1 recent-past unref
CNRM SSP5-8.5	Arc-1 future unref & dual-polar ref	Arc-1 future unref & Arctic ref	Arc-1 future unref & Arctic ref
NorESM historical	Arc-2 recent-past unref	Arc-2 recent-past unref	Arc-2 recent-past unref
NorESM SSP5-8.5	Arc-2 future unref & dual-polar ref	Arc-2 future unref & Arctic ref	Arc-2 future unref & Arctic ref
WACCM historical	Ant-1 recent-past unref	Ant-1 recent-past unref	Ant-1 recent-past unref
WACCM SSP5-8.5	Ant-1 future unref & dual-polar ref	Ant-1 future unref & Antarctic ref	Ant-1 future unref & Antarctic ref
MPI historical	Ant-2 recent-past unref	Ant-2 recent-past unref	Ant-2 recent-past unref
MPI SSP5-8.5	Ant-2 future unref & dual-polar ref	Ant-2 future unref & Antarctic ref	Ant-2 future unref & Antarctic ref

3 Storyline implementation, experimental design, and models

3.1 Common experiment protocol

We implement the storyline framework through global AMIP-style experiments where the atmosphere and land models are active and the SSTs and SICs are prescribed to daily fields from the storyline models CNRM, NorESM, WACCM, and MPI (Table 1). We employ three VR models, CESM, ICON, and MPAS, and carry out polar refined and unrefined experiments for the future and unrefined baseline experiments for the recent past (Table 2). The experiments are complimentary to those in Graff et al. (2026a), as we use the exact same models and grids and methodically aligned forcing protocols.

The refined grids were configured with the finest horizontal resolution poleward of 60° (or as close to 60° as technically feasible), a transitional region with intermediate resolution equatorward of the finest-resolution region, and relatively coarser resolution elsewhere (Graff et al., 2026a, their Fig. 1). The unrefined grids employed the coarsest resolution from the refined grids globally. Although the equatorward edge of the highest-resolution region was placed at similar latitudes in all models, the latitudinal extent of the transitional region varied more (Graff et al., 2026a, their Fig. 1 and Table S1). The finest and coarsest resolutions are approximately 10 km and 50 km in ICON and MPAS, and 28 km and 111 km in CESM. We ran CESM with dual-polar refinement and ICON and MPAS with one refined region per experiment, over the Arctic in the Arctic storyline experiments and over the Antarctic in the Antarctic experiments. See section 3.3 and Graff et al. (2026a) for further details.

The recent-past experiments were forced with SSTs and SICs for 2005–2014 from the CMIP6 historical runs from the respective storyline models (CNRM, NorESM, MPI, WACCM), and the future experiments with fields for 2090–2099 from the corresponding SSP5-8.5 runs (Fig. 1). The origin of the SST and SIC fields and the length of the experiments are two notable differences from Graff et al. (2026a), where the SSTs and SICs were from the fifth generation of the European Center for Medium-range Forecasts reanalysis (ERA5; Hersbach et al., 2020) and the experiments covered 30 years (1985–2014). The

https://doi.org/10.5194/egusphere-2026-5525
Preprint. Discussion started: 23 September 2026

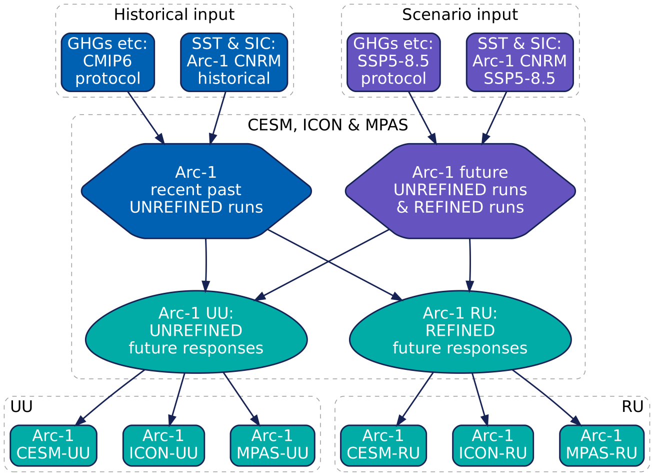

Figure 1. Schematic overview of the experimental set-up for the unrefined recent-past Arc-1 (CNRM) experiments (blue nodes) and the unrefined and refined future Arc-1 (CNRM) experiments (purple nodes). Also shown is the unrefined (UU) and refined (RU) future response fields that can be computed from this experiment set (green nodes). The CNRM historical and SSP5-8.5 are the official CMIP6 experiments.

restriction to 10 years here arises from the large computational and storage costs of associated with using multiple SST and SIC forcing fields, grids, and VR models (resulting in 36 different experiments; Table 2).

We prescribed time-varying forcings for greenhouse gases (CO_2, CH_4, N_2O, and Chlorofluorocarbons), ozone, and aerosols. For the recent-past runs, they were based on the CMIP6 historical forcings for 2005–2014, similar to in Graff et al. (2026a), while the forcings in the future runs were based on those for SSP5-8.5 for 2090–2099 (Fig. 1). For ICON and MPAS, some forcings could not be time varying due to technical restrictions, and in these cases climatologies representative of the recent-past or future conditions were used (see section 3.3 for further details).

In summary, we performed nine experiments for each storyline: an unrefined recent-past experiment and a refined and a unrefined future experiment with each of our three VR models (Fig. 1). Based on these experiments, we compute the *unrefined future responses* (UU) by differencing the unrefined future and recent-past experiments, and the *refined future responses* (RU) by differencing the refined future and unrefined recent-past experiments (large green ovals in Fig. 1), resulting in six future response fields per storyline (small green ovals).

3.2 Historical baseline sensitivity

The future period (2090–2099) used here corresponds to the last 10 years of the future period in L24 and W24 and the recent-past period (2005–2014) to the last 10 years of the historical period in L24. W24 used a mid-century period (1940–1969), to isolate the greenhouse-gas-driven response from ozone depletion in the late 20th century. We use a single recent-past period to optimize comparability between the Arctic and Antarctic results. We also note that our time periods are similar to those used in the Half a degree additional warming, prognosis and projected impacts (HAPPI) experiments (Mitchell et al., 2017).

https://doi.org/10.5194/egusphere-2026-5525
Preprint. Discussion started: 23 September 2026

Table 3. Standardized departures from the global-warming-scaled multi-model mean for DJFM for the Antarctic storyline predictors: sea-ice loss and SPV breakdown. The departures are given for the storylines and storyline models (column 1) for the 10-year and 30-year periods: 2090–2099−2005-2014 (columns 2–3) and 2070–2099−1985–2014 (column 4–5). The bottom row shows the difference between the Ant-2 and Ant-1 storyline models MPI and WACCM as percentage of the storyline difference in standardized units ($1.269 \times 2 = 2.583$); values exceeding 100% indicate that model signal (MPI−WACCM) exceeds the storyline signal and vice versa.

Storyline/	10-year periods		30-year periods	
storyline model	**sea ice**	**SPV**	**sea ice**	**SPV**
Ant-1	−1.269	−1.269	−1.269	−1.269
WACCM	−1.382	−0.968	−1.540	−0.883
Ant-2	1.269	1.269	1.269	1.269
MPI	1.069	−0.923	1.303	−0.223
MPI−WACCM (%)	96.60	1.800	112.0	26.00

Although harmonizing the historical period makes the experiment set more internally consistent, it also affects the Antarctic storyline models ability to represent storyline differences in the SPV predictor, due to the effect of ozone depletion during this later period (W24). We explore this by reassessing the storyline predictors standardized departures from the CMIP6 multi-model mean for the Antarctic storylines and storyline models for the new time periods (Table 3). By construction, the storyline departures are ±1.269 (−1.269 for Ant-1 and +1.269 for Ant-2) at the 80% joint confidence interval ellipse for both predictors (Mindlin et al., 2020). For the sea-ice-loss predictor, the storyline models closely match the storylines, with the difference between the models corresponding to about 100% of the storyline signal. For the SPV predictor, both storyline models simulate early breakdown (negative departures), and the model difference only represents 1.8% of the storyline difference for the 10-year periods. Thus, the Antarctic storyline models mainly reflects the sea-ice loss predictor for the time periods used here. We find similar results when extending the time periods to 30 years (comparing columns 2–3 and 4–5).

The fact that changing the historical baseline from a mid-century (W24) to a more recent period (present study) affects the extent to which the storyline models capture the changes in the storyline predictors, has important implications for model experiments that use storyline-model output to prescribe boundary conditions. Nevertheless, the experimental set-up employed here limits the storyline forcings to SST and SIC. Antarctic SST and SIC storylines for DJFM (Fig. 2), derived using the framework from W24 with data from the same models (Table S1) but for the 10-year periods used here, show that the characteristics of the near-surface temperature storylines from W24 (their Fig. 7) are captured in the SST storylines (Fig. 2a, e, and i), with Ant-1 warming more than Ant-2, particularly over the Southern Ocean. The Ant-1 and Ant-2 storyline models WACCM and MPI reflect the same warming difference, albeit somewhat stronger (Fig. 2b, f, and j). Consistent with the higher SSTs, the Ant-1 storyline and storyline model WACCM has more pronounced changes in SIC than the Ant-2 storyline and storyline model MPI (Fig. 2c–d, g–h, and k–l). These results are robust to the length of the time period, as extending the 10-year periods to 30 years

https://doi.org/10.5194/egusphere-2026-5525
Preprint. Discussion started: 23 September 2026

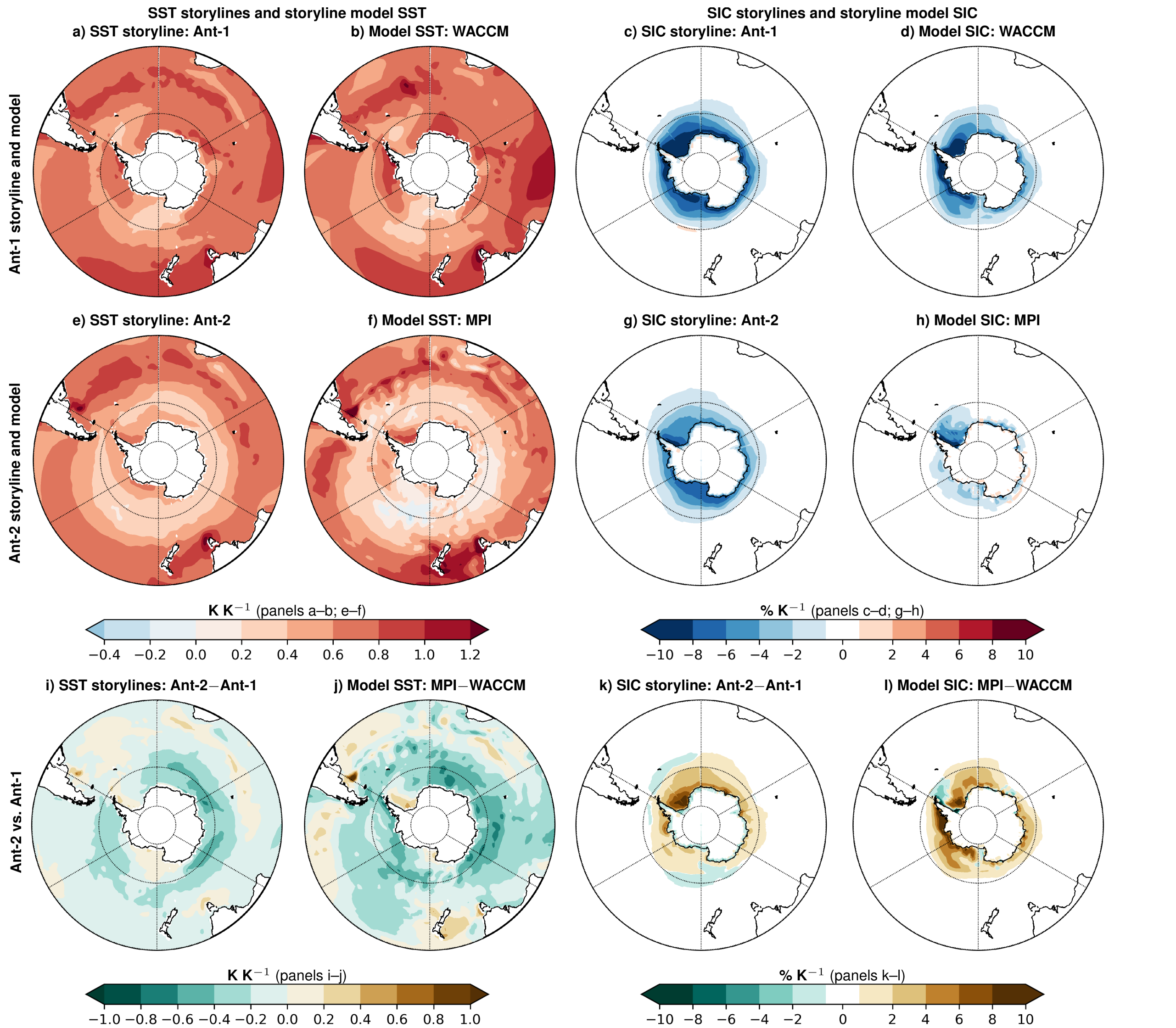

Figure 2. SST and SIC storylines for DJFM, derived using the framework from W24, shown with the SST and SIC fields from the storyline models (WACCM and MPI), and with the difference between the storylines (Ant-2 vs. Ant-1) and between the storyline models (MPI vs. WACCM) for 2090–2099−2005–2014. The top row shows the Ant-1 SST (a) and SIC (c) storylines with the SST (b) and SIC (d) field from the Ant-1 storyline model WACCM. The middle row shows (e–h) shows the same for Ant-2 and the Ant-2 storyline model MPI. The bottom row shows the difference between the Ant-2 and Ant-1 SST (i) and SIC (k) storylines and the difference between the storyline model's SST (j) and SIC (l) fields. The storylines are derived for the same CMIP6 models as in W24 (Table S1). The fields are scaled by global near-surface warming in line with W24. Units are K K^{-1} (a–b; e–f; i–j) and % K^{-1} (d–f; g–h; k–l).

yields similar results (Fig. S1). Note that we only consider SST and SIC storylines for the SH because of the important and confounding role of ozone depletion on the Antarctic storyline (SPV contributory) forcing.

https://doi.org/10.5194/egusphere-2026-5525
Preprint. Discussion started: 23 September 2026

3.3 The VR models

The CESM simulations were performed with version 2.2 (Danabasoglu et al., 2020), configured with version 6 of the Community Atmosphere Model (Lauritzen et al., 2018; Gettelman et al., 2019), version 5 of the Community Land Model (Lawrence et al., 2019) applied with prescribed satellite vegetation phenology, and the spectral element dynamical core. We ran the model with two grids: the unrefined grid, which has a globally uniform horizontal resolution of 1° (∼111 km); and the dual-polar refined grid which has a resolution of 0.25° (∼28 km) poleward of 60° in both hemispheres, 0.5° resolution in a transitional region between 60°N–45°N and 60°S–45°S, and 1° (∼111 km) resolution equatorward of 45°. The model was run with 58 hybrid-sigma levels with the model top at ~ 40 km in all cases.

All CESM experiments were spun up for one year. The unrefined experiments were initialized using the same initial condition as the ERA5-forced experiments (Graff et al., 2026a), namely the atmospheric state on 1. January 1984 from a 58-level CAM6 experiment representative for the recent past. The refined experiments were initialized from the end of the spin-up (1. January 1985) of the refined ERA5-forced experiments. Similar to the experiments in Graff et al. (2026a), time-varying GHGs, ozone and tropospheric aerosols in the recent-past and future experiments were taken from CESM2-WACCM experiments (Gettelman et al., 2019; Danabasoglu et al., 2020; Hoesly et al., 2018; van Marle et al., 2017) forced in line with the CMIP6 protocol for the historical experiment and for SSP5-8.5, respectively. See Wijngaard et al. (2025) for more details.

The ICON simulations were carried out with version 2.6.6. ICON has a non-hydrostatic dynamical core, exact local mass conservation, mass-consistent tracer transport, and is capable of flexible grid nesting (Zängl et al., 2015). The icosahedral-triangular Arakawa C grid allows for close to uniform grid spacing globally, and prevents polar singularities found with more traditional lat-lon grids. The unrefined simulations were run with the R3B5 resolution (∼52.6 km). The Arctic and Antarctic refined simulations were run with the R3B7 resolution (∼13.2 km) poleward of 57°N or 57°S, respectively. Due to the large difference between the refined and unrefined resolution, an intermediate nest using the R3B6 resolution (∼26.3 km) was implemented poleward of 50°S and 50°N. In the vertical, we used the same 90 vertical levels in all cases, with the model top being at 75 km.

All ICON simulations were initialized on 1 January 2004, followed by a one-year spin-up period. Transient greenhouse gas concentrations were prescribed according to the CMIP6 protocol for the historical (Meinshausen et al., 2017) and SSP5-8.5 experiments (O'Neill et al., 2016), respectively. Transient ozone concentrations were prescribed using the CMIP6 Chemistry–Climate Model Initiative (CCMI) dataset provided via input4MIPs (Hegglin et al., 2016). Aerosols were held constant in time, using the Tegen aerosol climatology (Tegen et al., 1997) for both historical and future simulations.

The MPAS simulations were carried out with version 7.3, configured with fully-compressible and non-hydrostatic dynamical core (Skamarock et al., 2012) and an unstructured centroidal Voronoi mesh, which has tiles of varying sizes and allows for smooth transitions between different sized tiles (Thuburn et al., 2009; Ringler et al., 2010). The unrefined simulations were run with 48 km resolution, and the Arctic and Antarctic refined simulations with a 46–12 km VR mesh with the finest resolution (12 km) applied poleward of 60°N or 60°S, respectively. Between 60°N/S and 30°N/S the tiles become progressively larger

https://doi.org/10.5194/egusphere-2026-5525
Preprint. Discussion started: 23 September 2026

and the resolution coarser, in order to transition smoothly from the 12 km to the 46 km resolution. We use the same 55 vertical geometric-height levels in all simulations.

All MPAS experiments were initialized on 1. January 1984 and spun up for one year. CO_2 was prescribed to time-varying annual-mean global-mean values from the CMIP6 historical and SSP5-8.5 scenario forcings (Cheng et al., 2022). Other GHGs (CH_4, N_2O, CFCs, and CCL_4) were prescribed to their global-mean and annual-mean concentrations of 2005. Aerosols and ozone concentrations are prescribed from monthly and daily climatologies, respectively.

3.4 Data from CMIP6 models

For the storyline models CNRM (Seferian, 2018b; Voldoire, 2019e), NorESM (Bentsen et al., 2019a, b), WACCM (Danabasoglu, 2019c, d), and MPI (Wieners et al., 2019b, a), we use daily-mean SST and SIC and monthly-mean near-surface, 850-hPa, and 250-hPa temperature, near-surface wind speed, 850-hPa and 250-hPa zonal wind, sea level pressure, total precipitation rate, total cloud cover, and near-surface specific humidity. For the Antarctic SST and SIC storylines (Fig. 2), we use the monthly-mean SST and SIC fields from 32 different models (listed in Table S1). For consistency with the VR-model experiments, we use data from the CMIP6 historical and SSP5-8.5 experiments for years 2005–2014 (historical) and 2090–2099 (SSP5-8.5). We also use 1985–2014 and 2070–2099 to assess the sensitivity of the results to the length of the time period.

4 Summary metrics

To quantify the influence of the storyline model forcing, the VR model, and the resolution on our results, we designed three metrics: the storyline influence, the VR-model influence, and the resolution influence. The metrics are dissimilarity estimates that build upon the spatial pattern correlation coefficients for the future responses and are defined as the mean deviation from a perfect correlation due to different factors (storyline, model, or resolution):

$$\mu = \frac{1}{N} \sum_{(x,y)\in P} (1 - \rho(x,y)) \tag{1}$$

where μ is the mean dissimilarity, P is a paired set of future responses, N is the number of pairs, and ρ is the cosine-weighted Pearson's spatial pattern correlation coefficient (for each pair of future responses). The mean dissimilarity is large when the future responses in P are dissimilar and poorly correlated. Conversely, the mean dissimilarity is small when the future responses are similar and highly correlated.

The pattern correlation coefficients are computed for mid- and high-latitude future responses ($\geq 40°$N for the Arctic storyline experiments and $\geq 30°$S for the Antarctic experiments), for consistency with L24 and W24. The coefficients are cosine weighted to account for the grid-cell area varying with latitude. All data are re-gridded to a common 1×1 degree regular grid in the horizontal as a pre-processing step. We chose this resolution because it approximately corresponds to the resolution of the coarsest model experiment (e.g. Liang et al., 2021; Wills et al., 2024; Sun et al., 2026).

As shown in Fig. 1, our VR-model experiments yield six future responses for each storyline (UU and RU responses for CESM, ICON, and MPAS), resulting in 12 future responses, both for the Arctic and for the Antarctic storyline experiments.

https://doi.org/10.5194/egusphere-2026-5525
Preprint. Discussion started: 23 September 2026

For each experiment set (Arctic or Antarctic), we compute pattern correlation coefficients between all 12 responses and derive the metrics from subsets of these correlation coefficients. Each metric uses a unique set of future response pairs:

– *The storyline influence* (μ_s) is the mean deviation from a perfect correlation due to the across-storyline correlation coefficients (Arc-1 versus Arc-2 or Ant-1 versus Ant-2) for the same VR model and the same resolution. For two contrasting storylines S-1 and S-2, this can be generalized as:

$$P_s = \{(\text{S-1 CESM-UU, S-2 CESM-UU}), (\text{S-1 CESM-RU, S-2 CESM-RU}), (\text{S-1 ICON-UU, S-2 ICON-UU}), (\text{S-1 ICON-RU, S-2 ICON-RU}), (\text{S-1 MPAS-UU, S-2 MPAS-UU}), (\text{S-1 MPAS-RU, S-2 MPAS-RU})\} \quad (2)$$

Where S-1 and S-2 are Arc-1 and Arc-2 or Ant-1 and Ant-2.

– *The VR-model influence* (μ_m) is the mean deviation from a perfect correlation due to the across-model correlation coefficients (CESM versus ICON, CESM versus MPAS, and ICON versus MPAS) for the same storyline and resolution:

$$P_m = \{(\text{S-X CESM-UU}, \text{S-X ICON-UU}), (\text{S-X CESM-UU}, \text{S-X MPAS-UU}), (\text{S-X ICON-UU}, \text{S-X MPAS-UU}), (\text{S-X CESM-RU}, \text{S-X ICON-RU}), (\text{S-X CESM-RU}, \text{S-X MPAS-RU}), (\text{S-X ICON-RU}, \text{S-X MPAS-RU})\} \quad (3)$$

where S-X $\in \{\text{Arc-1}, \text{Arc-2}\}$ or S-X $\in \{\text{Ant-1}, \text{Ant-2}\}$.

– *The resolution influence* (μ_r) is the mean deviation from a perfect correlation due to the across-resolution correlation coefficients (UU versus RU) for the same storyline and model:

$$P_{r,Arc} = \{(\text{S-X ICON-UU}, \text{S-X ICON-RU}), (\text{S-X ICON-UU}, \text{S-X ICON-RU}), (\text{S-X MPAS-UU}, \text{S-X MPAS-RU})\} \quad (4)$$

In summary, the storyline, VR model, or resolution influence is large when the relevant across-storyline, across-model, or across-resolution pattern correlation coefficients are low. Hence, the spatial structure of the future responses are distinct and depend on the choice of storyline (i.e., SSTs and SICs fields), VR model, or resolution. Small values signify that the future responses are highly correlated and the influence of the SST and SIC forcing, VR model, or resolution is low.

In addition to quantifying the influence of the SST and SIC fields on the VR-model results (the storyline influence), we also quantify the spatial difference between the future responses from the storyline models themselves in terms of a separate metric:

– *The forcing-model contrast* (μ_f) quantifies how much the across-forcing-model (or across-storyline-model) correlation coefficient deviates from 1. Unlike the other metrics, the forcing-model contrast only uses a single pattern correlation value per storyline pair:

$$P_{f,Arc} = \{(\text{Arc-1 CNRM-10}, \text{Arc-2 NorESM-10})\} \quad (5)$$

$$P_{f,Ant} = \{(\text{Ant-1 WACCM-10}, \text{Ant-2 MPI-10})\} \quad (6)$$

where $P_{f,Arc}$ and $P_{f,Ant}$ is the forcing-model contrast for the Arctic and Antarctic storyline models and "-10" indicates that the future responses are computed from the 10-year periods (2005–2014 and 2090–2099; section 3). Note that

https://doi.org/10.5194/egusphere-2026-5525
Preprint. Discussion started: 23 September 2026

we deliberately use the term "contrast" rather than "influence" for this metric to distinguish between the influence of the storyline forcing on the VR-model results (the storyline influence) and the difference between storyline models themselves (the forcing-model contrast).

In addition to the mean metrics, we also consider the spread (σ) for the storyline, VR-model, and resolution influence, computed using the following equation with the pairs defined in equation 2–4:

$$\sigma = \sqrt{\frac{1}{N} \sum_{(x,y) \in P} [(1 - \rho(x,y)) - \mu]^2} \tag{7}$$

5 Results for Arctic storyline experiments

In this section, we first explore the Arctic VR-model storyline experiments, assessing whether they capture the known storyline characteristics from L24 and whether they remain distinct when we account for the full range of solutions across models and resolutions. We focus on three target variables from L24: near-surface temperature, total precipitation rate, and 850-hPa zonal wind. We emphasize the season for which the storylines were designed (MJJASO), but also put the results into broader context by including the four standard three-month seasons December–February (DJF), March–May (MAM), June–August (JJA), and September–November (SON). Then, we apply the summary metrics to a wider range of fields to quantify the influence of the storyline, VR model, and resolution, and to explore the forcing-model contrast.

Our analysis is based on 16 different future response fields (see Table S2 for a detailed overview). For Arc-1, two of them are for the storyline model CNRM, computed by differencing its SSP5-8.5 and CMIP6 historical experiments for the 10-year and 30-year periods (section 3). We refer to these responses as Arc-1 CNRM-10 and Arc-1 CNRM-30. The remaining six are the UU (unrefined future−unrefined recent past) and RU (refined future−unrefined recent past) responses, computed from the Arc-1 VR-model experiments: Arc-1 CESM-UU, Arc-1 ICON-UU, Arc-1 MPAS-UU, Arc-1 CESM-RU, Arc-1 ICON-RU, and Arc-1 MPAS-RU (Fig. 1). The Arc-2 future responses are defined in the same way, but using the NorESM SSP5-8.5 and CMIP6 historical runs for the storyline-model responses (Arc-2 NorESM-10/30) and the VR-model experiments forced with SSTs and SICs from NorESM for the UU and RU responses (Arc-2 CESM/ICON/MPAS-UU/RU). For consistency with L24, we normalize the future responses by the respective experiments' global-mean near-surface warming and only include latitudes $\geq 40°$N. For 850-hPa fields, we mask out sub-surface grid points.

5.1 The extended NH summer season

We find the future changes in near-surface temperature during MJJASO to be consistent with L24, with CNRM characterized by strong warming over the Arctic Ocean, including the Barents-Kara Seas, and weaker warming over land (Fig. 3a). Conversely, NorESM has weaker warming over the Arctic Ocean (including the Barents-Kara Seas) and stronger warming over the continents (Fig. 3c). These features are also clearly seen from the difference between the Arc-2 and Arc-1 responses for both the 10-year and 30-year time periods (Fig. S2c–d), indicating that this is a robust result; however, only the largest differences are significant and the continental changes are more significant for the longer time period (Fig. S2d).

https://doi.org/10.5194/egusphere-2026-5525
Preprint. Discussion started: 23 September 2026

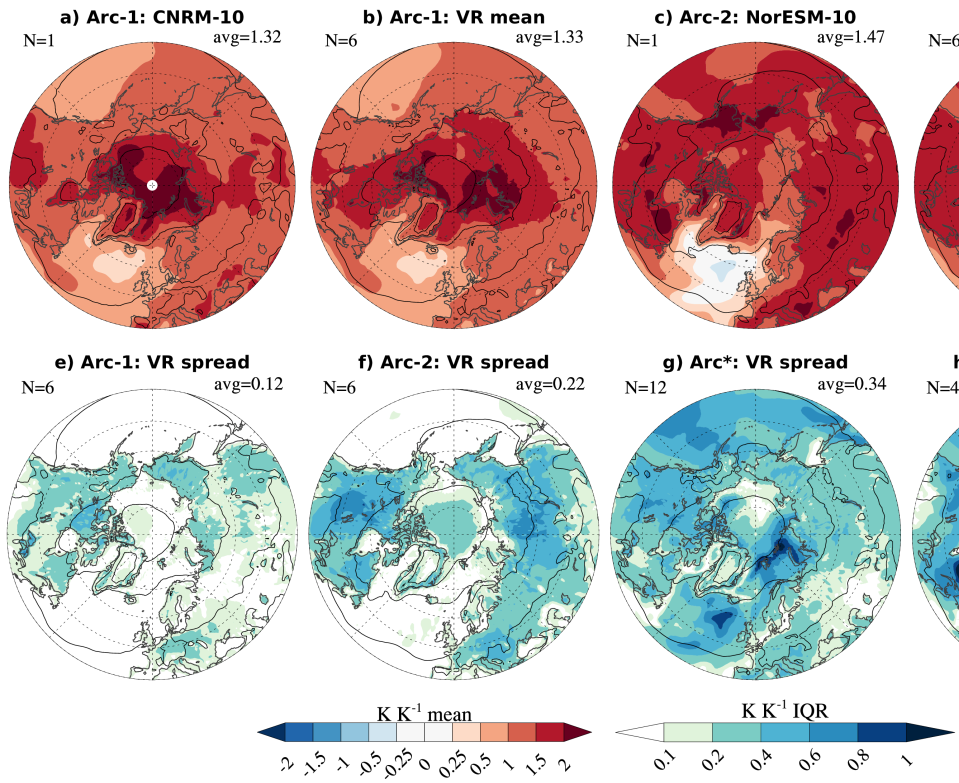

Figure 3. Future change in near-surface temperature during MJJASO for the Arc-1 storyline model (CNRM-10; a), the Arc-1 VR-model mean (Arc-1 CESM/ICON/MPAS-UU/RU; b), the Arc-2 storyline model (NorESM-10; c), and the Arc-2 VR-model mean (Arc-2 CESM/ICON/MPAS-UU/RU; d). Also shown is the IQR (spread) for the Arc-1 (e), Arc-2 (f), and combined Arc-1 and Arc-2 (g) VR-model responses, and of the combined storyline-model responses for both time periods (CNRM-10/30 and NorESM-10/30; h). N denotes the number of response fields in each panel. Future responses are defined in Table S2 and normalized by global near-surface warming. Units are $K\,K^{-1}$.

The VR models reproduce the characteristic features of Arc-1 and Arc-2 with relatively strong Arctic-Ocean warming and relatively weak continental warming in Arc-1 and vice versa in Arc-2 (Fig. 3b and d). Compared to the storyline models, the VR models have a more muted response over the central Arctic ocean and a stronger response over the northernmost parts of the continents for Arc-1, while for Arc-2 they have more muted warming over the continents and more spatially extensive warming over the Arctic Ocean (Fig. 3a–d). The VR models generally match the storyline-model warming most closely over the open ocean but differ more over sea ice and land (Fig. 3a–d), as expected from the experimental design (section 3).

The VR models exhibit the most pronounced spread over the continents for both Arc-1 and Arc-2 (Fig. 3e–f). The diversity over the continents is also reflected in the spread across the combined Arc-1 and Arc-2 VR-model responses (Fig. 3g). Over the ocean and sea-ice covered regions, the combined VR-model spread strongly resembles the combined storyline-model spread (Fig. 3h), highlighting differences between the storyline models over the Barents-Kara Seas and the North Atlantic

https://doi.org/10.5194/egusphere-2026-5525
Preprint. Discussion started: 23 September 2026

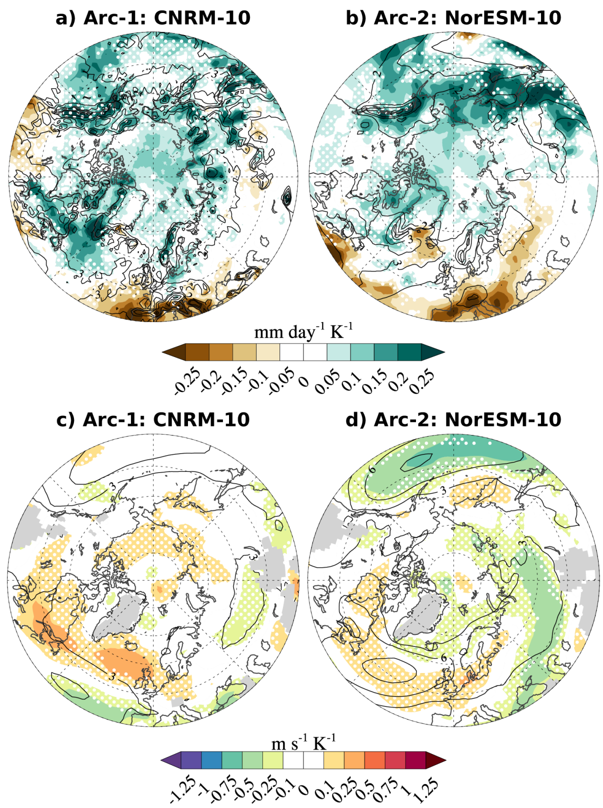

Figure 4. Future changes in total precipitation rate (a–b) and 850-hPa zonal wind (c–d) during MJJASO for the Arc-1 (a and c) and Arc-2 (b and d) storyline models (CNRM-10 and NorESM-10). Future responses are defined in Table S2. Panel titles and normalization are as in Fig. 3. White dots indicate changes that are *not significant* at the 95% level according to a two-sided T-test. Units are m s^{-1} K^{-1} (a–b) and mm day^{-1} K^{-1} (c–d).

Warming Hole (NAWH). The latter reflects that NorESM has a strong NAWH with a small cooling patch, while CNRM has a more moderate cooling deficit. The NAWH has been tied to increased freshwater inflow and the subsequent weakening of the Atlantic Meridional Overturning Circulation (Keil et al., 2020; Liu et al., 2020; Weijer et al., 2020).

Although the main characteristics of the Arctic storylines are captured by both the storyline models and VR models for near-surface temperature (Fig. 3 and S2a–d), results are less clear for precipitation and 850-hPa zonal wind (Fig. 4 and S2e–l). L24 found Arc-2 to be drier over the northernmost parts of the NH continents and the North Atlantic and wetter over the eastern and northern part of the North Pacific (their Fig. 5). Here, we find NorESM to be drier than CNRM in patches over the North Atlantic and western Eurasia, but differences are weak and mostly insignificant over central and eastern Russia and the North Pacific (Fig. 4a–b and S2e–h). For 850-hPa zonal wind, L24 found a stronger poleward shift over the North Atlantic and a stronger weakening over the North Pacific for Arc-2 (their Fig. 4). We find the storyline models capture these characteristics relatively well for the 10-year periods over the North Pacific, albeit with a more basin-wide weakening (Fig. 4c–d and S2i–l).

https://doi.org/10.5194/egusphere-2026-5525
Preprint. Discussion started: 23 September 2026

Over the North Atlantic NorESM has a weak and insignificant equatorward shift (Fig. 4d). The difference between NorESM and CNRM for the 10- and 30-year periods (Fig. S2k–l) show that the North-Atlantic response is sensitive to the time period and that only the longer time period reproduces the results from L24. Hence, the storyline models do not capture the storyline characteristics for precipitation and zonal wind as clearly as for near-surface temperature.

We can compare the future change patterns more objectively in terms of Pearson's spatial pattern correlation coefficients. We consider the full set of future responses (Table S2) for MJJASO near-surface temperature first. After regridding all data to a common 1×1 degree regular grid in the horizontal as a pre-processing step, we compute the correlation coefficients along the latitude and longitude dimensions, applying a standard cosine weighting to account for the grid-cell area varying with latitude. The responses are positively correlated in all cases with values of 0.48 or higher, indicating a consistent degree of agreement across all solutions (Fig. 5). The agreement is considerably higher for the within-storyline coefficients (Arc-1 versus Arc-1 and Arc-2 versus Arc-2 coefficients; upper-left and lower right quadrants) compared to the across-storyline coefficients (Arc-1 versus Arc-2 coefficients; upper-right/lower-left quadrants). This means that the Arc-1 responses tend to more closely resemble other Arc-1 responses than Arc-2 responses and vice versa and suggests that the Arctic-storyline experiments can be considered *separable* (or distinct) for this field and season.

The within-storyline differences tend to be small for Arc-1 with values ranging from 0.84 to 0.99 (excluding the diagonal line; Fig. 5). For Arc-2, results vary a bit more, with values ranging from 0.76 to 0.97. This is in line with the Arc-1 warming being more dominated by the Arctic Ocean, a region which is constrained by the prescribed lower-boundary forcing, while the Arc-2 warming is more dominated by the Northern Hemisphere (NH) continents where the warming is calculated by the respective model's freely running land component. Consistently, VR-model spread is larger for Arc-2 than Arc-1 with the main difference over the continents (Fig. 3e–f). Furthermore, the Arc-2 storyline model NorESM is somewhat more strongly correlated to CESM than to ICON and MPAS (Fig. 5). This is likely related to CESM and NorESM being relatively similar models, sharing the same land and sea-ice models and having similar atmosphere models (Seland et al., 2020). ICON and MPAS are, on the other hand, somewhat more strongly correlated to each other.

Figures 3 and 5 show that key storyline characteristics are well captured for near-surface temperature for MJJASO and that the storylines are separable with high values for the within-storyline correlation coefficients and lower values for the across-storyline coefficients. Next, we investigate separability more formally by assessing whether the distributions of within-storyline and across-storyline pattern correlation coefficients are significantly different. Furthermore, we explore whether the separability of the Arctic storylines holds for other seasons and the extent to which precipitation and zonal wind are separable.

5.2 Separability of Arctic storyline experiments

We assess whether our storyline experiments are separable for a specific variable and season by evaluating whether the distribution of within-storyline correlation coefficients (e.g. upper-left quadrant in Fig. 5) is *significantly different* from the respective distribution of across-storyline correlation coefficients (e.g. upper-right quadrant in Fig. 5) according to the two-sided Mann-Whitney U test. Note that for the within-storyline coefficients, we only include the below-diagonal values, thus excluding the diagonal line and repeated coefficients.

https://doi.org/10.5194/egusphere-2026-5525
Preprint. Discussion started: 23 September 2026

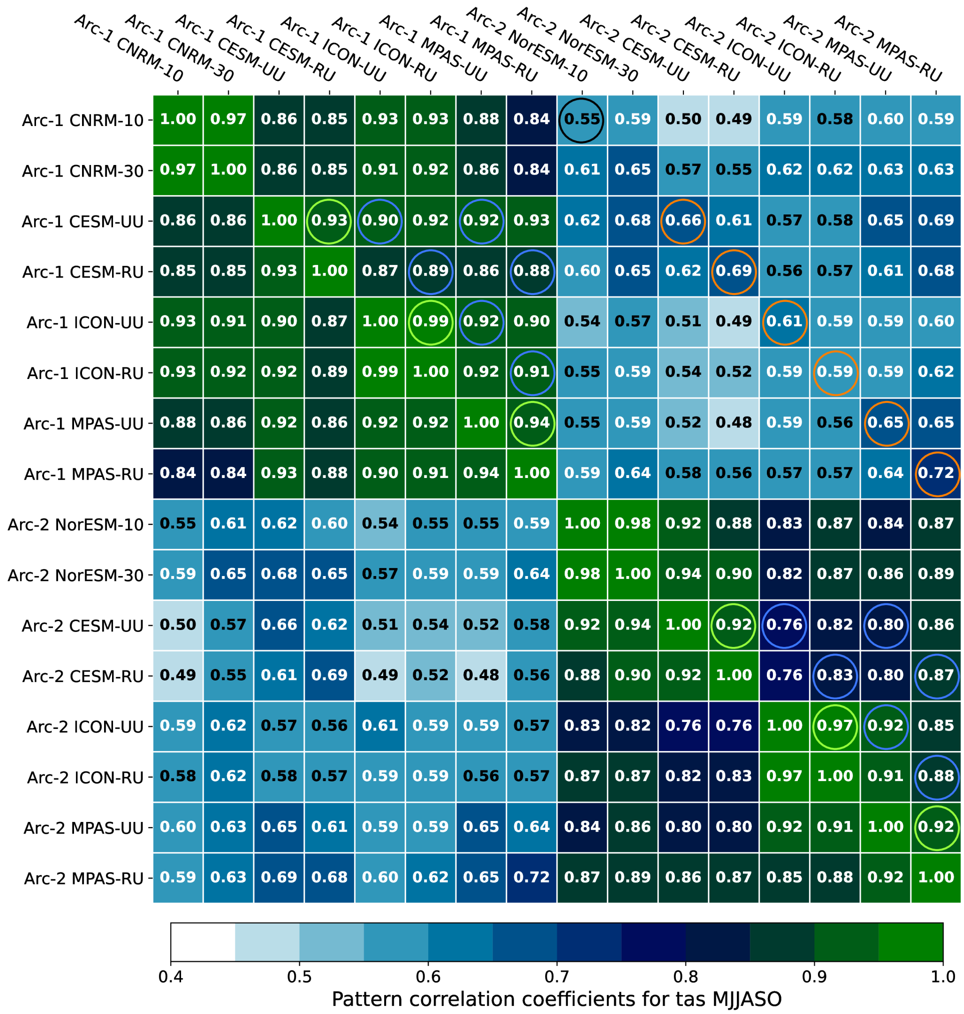

Figure 5. Pattern correlation matrix for future changes in near-surface temperature (tas) during MJJASO for Arctic storyline models (Arc-1 CNRM-10/30 and Arc-2 NorESM-10/30) and VR models (Arc-1/Arc-2 CESM/ICON/MPAS-UU/RU). Orange, blue, green, and black circles highlight the coefficients we use to estimate the storyline influence (equation 1 and 2), VR-model influence (equation 1 and 3), resolution influence (equation 1 and 4), and the forcing-model contrast (equation 1 and 5), respectively. Future responses are defined in Table S2. The correlation coefficients are computed for latitudes $\geq 40°$N and cosine weighted. Units are dimensionless.

For MJJASO near-surface temperature (Fig. 6a), the within-storyline distributions for Arc-1 (yellow box) and Arc-2 (teal box) are both significantly different from the across-storyline distribution (grey box), as indicated by the magenta asterisk. Thus, we consider Arc-1 and Arc-2 to be separable for this variable and season. The separation between the within- and across-storyline distributions is particularly pronounced during MJJASO and JJA, when the Arc-1 and Arc-1 distributions are located entirely above the across-storyline distribution, consistent with Fig. 5. The across-storyline values are lower for JJA than

https://doi.org/10.5194/egusphere-2026-5525
Preprint. Discussion started: 23 September 2026

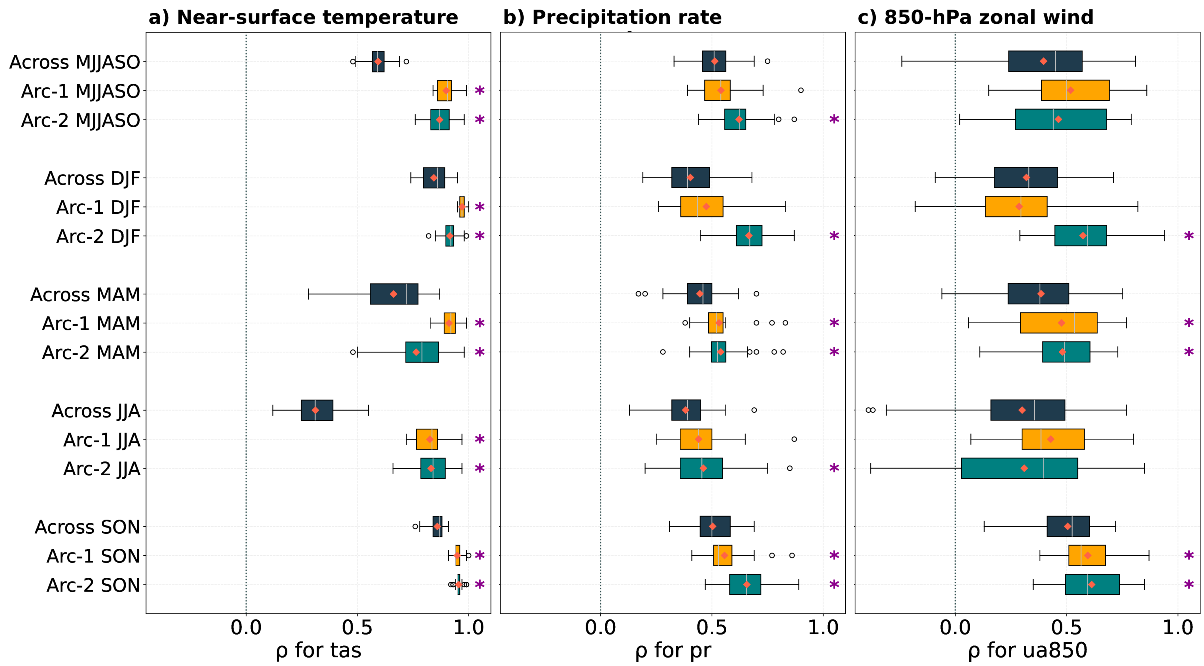

Figure 6. Seasonal distributions of pattern correlation coefficients (ρ) for future changes in the Arctic storyline-model and VR-model experiments (Arc-1/Arc-2 CNRM/NorESM-10/30 and Arc-1/Arc-2 CESM/ICON/MPAS-UU/RU; Table S2) for near-surface temperature (tas; a), total precipitation rate (pr; b), and 850-hPa zonal wind (ua850; c). Distributions are shown for MJJASO, DJF, MAM, JJA, and SON for the across-storyline (dark gray), Arc-1 (yellow), and Arc-2 (teal) coefficients. The across-storyline distributions correspond to the upper-right/lower-left quadrants of the respective correlation matrices and the Arc-1 and Arc-2 distributions to the unique off-diagonal correlation coefficients of the upper-left (Arc-1) and lower-right (Arc-2) quadrants. The boxes show the IQR and the whiskers extend to the furthest data point or, in the case of outliers (open circles), to 1.5 times the IQR from the box edge. The vertical black dotted line indicates zero. Magenta asterisks indicate significant differences ($p < 0.05$) between the Arc-1 or Arc-2 and across-storyline distributions according to a two-sided Mann-Whitney U test. The correlation coefficients are computed for latitudes $\geq 40°$N and cosine weighted. Units are dimensionless.

MJJASO, resulting in a larger separation between the across- and within-storyline distributions for this season. While the three distributions are more similar during the other seasons (DJF, MAM, and SON), Arc-1 and Arc-2 are still significantly different, and thus separable from the across-storyline distribution, in all cases. During DJF and MAM, Arc-1 differs more from the across-storyline distribution than Arc-2, with the Arc-1 interquartile range (IQR) consistently placed above the across-storyline IQR.

The storylines are not as distinct or as highly correlated for precipitation or 850-hPa zonal wind (Fig. 6b–c). The pattern correlation coefficients are positive in all cases for precipitation (Fig. 6b), but they are generally smaller with larger spread and more outliers compared to for temperature. Still, Arc-2 is separable for all seasons and Arc-1 for MAM and SON. The relatively lower correlation coefficients for this field are likely linked to precipitation having substantial variability throughout

https://doi.org/10.5194/egusphere-2026-5525
Preprint. Discussion started: 23 September 2026

the midlatitudes in the VR models, with the Arc-1, Arc-2, and combined Arc-1 and Arc-2 VR-model spread exceeding the storyline model spread for all seasons and latitudes, except north of 75°N during DJF and MAM (Fig. S3f–j).

The range of values is larger still for zonal wind, which even features anti-correlated future response fields (Fig. 6c). Arc-2 DJF represents the case where the within-storyline distribution is most distinct from the across-storyline distribution with almost non-overlapping IQRs (Fig. 6c). Arc-1 and Arc-2 are also separable for MAM and SON, but differences between the across- and within-storyline distributions are smaller for these seasons. As for precipitation, we find substantial diversity in the future responses for zonal wind with Arc-1, Arc-2, and combined Arc-1 and Arc-2 VR-model spread mostly exceeding the storyline-model spread (Fig. S3k–o). The difference is most pronounced during DJF, when the Arc-2 VR-model spread is especially large.

The relatively lower correlation coefficients and more pronounced spread for precipitation and zonal wind are likely due to these fields being less effectively constrained by the storyline (SST and SIC) forcing and to being characterized by stronger internal variability than near-surface temperature. For zonal wind, the latter is even reflected in the future responses for the storyline models, as we find different changes over the North Atlantic for the 10- and 30-year periods (Fig. S2i–l).

5.3 Arctic summary metrics

Below, we summarize our results in terms of the four summary metrics defined in section 4: the storyline influence, the VR-model influence, the resolution influence, and the forcing-model contrast. The first three are based on the VR-model results, while the fourth metric is based on the storyline (forcing) models.

The storyline influence is an estimate of how much the across-storyline correlation coefficients for the same model and resolution (values with orange circles in Fig. 5) deviate from a perfect correlation. Similarly the VR-model and resolution influence estimate the mean deviation from a perfect correlation due to the across-model coefficients for the same storyline and resolution (values with blue circles in Fig. 5) and the across-resolution coefficients for the same storyline and model (values with green circles in Fig. 5), respectively.

The metrics range between 0 and 2, with the smallest value only attained when all future response pairs are perfectly correlated and the largest when all pairs are perfectly anti-correlated (equation 1). Small values signify that the future response fields that go into the across-storyline, across-model, or across-resolution are strongly correlated. In other words, the responses are similar regardless of the choice of storyline, model, or resolution; hence the *influence* of these factors is weak. Conversely, large values signify that the future responses that go into the across-storyline, across-model, or across-resolution coefficients are weakly correlated and that the future responses are more sensitive to the choice of storyline, model, or resolution.

The forcing-model contrast is computed from a single correlation coefficient (black circle in Fig. 5). Large values means that the storyline models' future responses are weakly correlated and that the models are dissimilar. Small values means that the responses are strongly correlated and that the future responses are similar regardless of whether it is computed from NorESM or CNRM data.

Figure 7 shows the four metrics for nine variables: near-surface, 850-hPa, and 250-hPa temperature, near-surface wind speed, 850-hPa zonal wind, sea level pressure, precipitation, total cloud cover, and near-surface humidity across seasons. A common

https://doi.org/10.5194/egusphere-2026-5525
Preprint. Discussion started: 23 September 2026

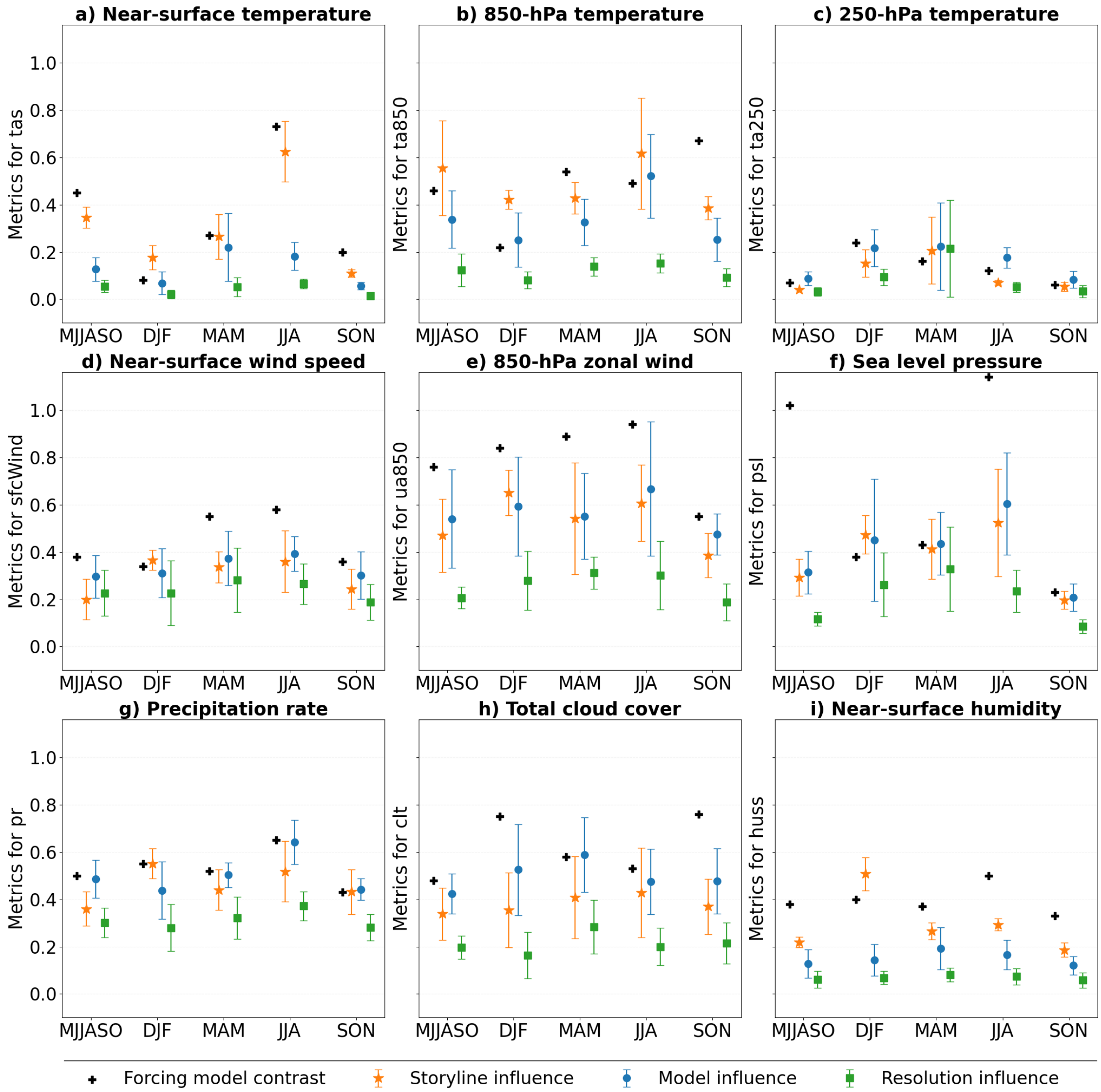

Figure 7. Metrics for the Arctic storyline-model and VR-model experiments for the storyline influence (equation 1 and 2; orange stars), VR-model influence (equation 1 and 3; blue dots), resolution influence (equation 1 and 4; green squares), and forcing-model contrast (equation 1 and 5; black plus signs) for near-surface, 850-hPa, and 250-hPa temperature (tas, ta850, ta250; a–c), near-surface wind speed (sfcWind; d), 850-hPa zonal wind (ua850; e), sea level pressure (psl; f), total precipitation rate (pr; g), total cloud cover (clt; h), and near-surface specific humidity (huss; i) for MJJASO, DJF, MAM, JJA, and SON. For the influence metrics, markers denote the mean and vertical bars ± one standard deviation (equation 7). The forcing-model contrast is based on a single pattern correlation coefficient, and the marker shows this value. The correlation coefficients the metrics are based on are computed for latitudes $\geq 40°$N and cosine weighted. Units are dimensionless.

https://doi.org/10.5194/egusphere-2026-5525
Preprint. Discussion started: 23 September 2026

feature is that the mean resolution influence (green squares) tends to be smaller than the storyline influence (orange stars) and VR-model influence (blue dots). This result is particularly robust for near-surface and 850-hPa temperature, 850-hPa zonal wind, and near-surface humidity (Fig. 7a, b, e, and i), where the vertical bars (± one standard deviation) show little to no overlap with those of the other metrics. While the resolution tends to exert the weakest influence, it matters more for wind, precipitation, cloud cover, and sea level pressure than for the near-surface temperature and humidity fields (Fig. 7a, d, e, g, h, f and i). The stronger resolution dependence of wind, sea level pressure, precipitation, and cloud cover indicates that these fields are more sensitive to model resolution than thermodynamic variables such as temperature and humidity. The resolution influence generally exhibits weak seasonal variations, with the exception of it being somewhat stronger during spring for 250-hPa temperature, sea level pressure, and the cloud cover (Fig. 7c, f, and h). In the former case, the resolution influence is comparable to the storyline and VR-model influence.

The mean storyline influence exceeds the mean VR-model and resolution influence for near-surface temperature, 850-hPa temperature and near-surface humidity (Fig. 7a–b and i), indicating that the storyline forcing (prescribed SST and SIC fields) dominates in these cases. The difference is particularly robust for near-surface temperature during JJA and MJJASO and for near-surface humidity during DJF. The former is consistent with the storylines being designed to maximize the spread in plausible Arctic temperature responses for the extended summer season (L24), and shows that our VR-model runs successfully capture this spread in summer, thereby maximizing the influence of the storyline on Arctic near-surface temperature. The storyline influence is also large during JJA and MJJASO for 850-hPa temperature, but the spread is larger and partly overlaps with that of the VR-model influence. For the other fields (Fig. 7c–h), the storyline influence is less dominant as the VR-model and resolution influence matter more.

The mean VR-model influence generally lies between the storyline and the resolution influence, however, the spread can be substantial. For 250-hPa temperature and clouds (Fig. 7c and h), the mean VR-model influence slightly exceeds the storyline influence in all seasons. The uncertainty intervals of the model and storyline influence are however only clearly separated for 250-hPa temperature during JJA. For wind speed, sea level pressure, and precipitation (Fig. 7d–g), the mean VR-model influence is generally comparable or slightly larger than the storyline influence, except during DJF, when it is somewhat weaker. The relatively strong VR-model influence on precipitation and clouds (Fig. 7g–h) is consistent with these fields depending more strongly on physical parameterizations and being less constrained by the prescribed SST and SIC fields.

The forcing-model contrast varies notably between fields and seasons. While it is mostly within the range of the other metrics, it tends to be larger than the storyline influence for wind (Fig. 7d–e) and near-surface humidity (Fig. 7i; except during DJF), indicating that the forcing models are weakly correlated and that their differences are not entirely captured in the VR-model experiments. For sea level pressure, we even find values exceeding 1 for MJJASO and JJA, indicating that the storyline models are weakly anti-correlated (Fig. 7f). For near-surface temperature, the forcing-model contrast is within the spread of the relatively large storyline influence during JJA.

The influence metrics tend to be particularly small for near-surface temperature, 250-hPa temperature, and near-surface humidity (Fig. 7a, c, and i), implying a generally robust climate change signal across the simulations. This is expected for near-surface temperature, as changes in this variable tend to have higher signal-to-noise ratio compared to more dynamical fields

https://doi.org/10.5194/egusphere-2026-5525
Preprint. Discussion started: 23 September 2026

like precipitation (e.g., Deser et al., 2012b), but is perhaps more surprising for 250-hPa temperature. Given the experimental design of the VR-model experiments, near-surface humidity is expected to be more constrained by the lower-boundary forcing, similar to near-surface temperature.

Overall, a clear distinction emerges between thermodynamic and dynamical variables. Near-surface temperature, lower-tropospheric temperature, and humidity are primarily controlled by the imposed storyline forcing, whereas precipitation, cloud cover, winds, and sea level pressure exhibit a larger dependence on the choice of VR model and, to a lesser extent, model resolution. Resolution effects are generally secondary but become increasingly important for dynamical and hydrological fields.

6 Results for Antarctic storyline experiments

We consider 16 future response fields for the Antarctic (Table S3), as for the Arctic (section 5). For Ant-1, these consist of the 10-and 30-year future responses from the storyline model WACCM (Ant-1 WACCM-10/30) and the VR-model UU and RU responses from experiments forced with WACCM SST and SIC fields (Ant-1 CESM/ICON/MPAS-UU/RU). Similarly, for Ant-2, we consider 10- and 30-year the future responses from the storyline model MPI (Ant-2 MPI-10/30) and the VR-model UU and RU responses from the experiments forced with SSTs and SICs from MPI (Ant-2 CESM/ICON/MPAS-UU/RU). We analyze the same variables as in section 5, with consistent normalization and masking of sub-surface grid points. For consistency with W24, we include latitudes $\geq 30°$S and highlight DJFM.

6.1 The extended SH summer season

We first consider the extended SH summer season (DJFM) for which the Antarctic storylines were designed. Future changes in near-surface temperature in the storyline models are consistent with W24 (their Fig. 7) with relatively uniform and similar warming in the 30°S–50°S band, and more contrasting changes further south where WACCM warms more than MPI (Fig. 8a and c). This is in line with Ant-1 being the storyline with large future changes in sea-ice extent (Table 1). MPI, which represents the storyline with weaker future changes in sea-ice extent, consistently has a more muted warming surrounding Antarctica, particularly in the Ross-Sea region and north of Wilkes Land. The results are very similar for the 10- and 30-year periods (Fig. S4c–d).

The Ant-1 and Ant-2 VR-model experiments (Fig. 8b and d) correspond well to the respective storyline models (Fig. 8a and c). This is as expected, given that the SH mid- and high-latitudes are largely ocean covered, rendering the SST and SIC forcing more influential than in the NH. As in the NH, the largest differences appear over the continents, in line with the land models being active. For example, the Ant-1 VR-model experiments are colder than WACCM over Antarctica (Fig. 8a–b).

Antarctica is also where the VR-model runs exhibit the most pronounced spread (Fig. 8e–f). This is also reflected in the combined (Ant-1 and Ant-2) VR-model spread, which additionally captures the contrasting SST forcings and is very similar to the combined storyline-model spread (Fig. 8g–h). In the sea-ice regions, the spread is largest in the Indian Ocean sector.

https://doi.org/10.5194/egusphere-2026-5525
Preprint. Discussion started: 23 September 2026

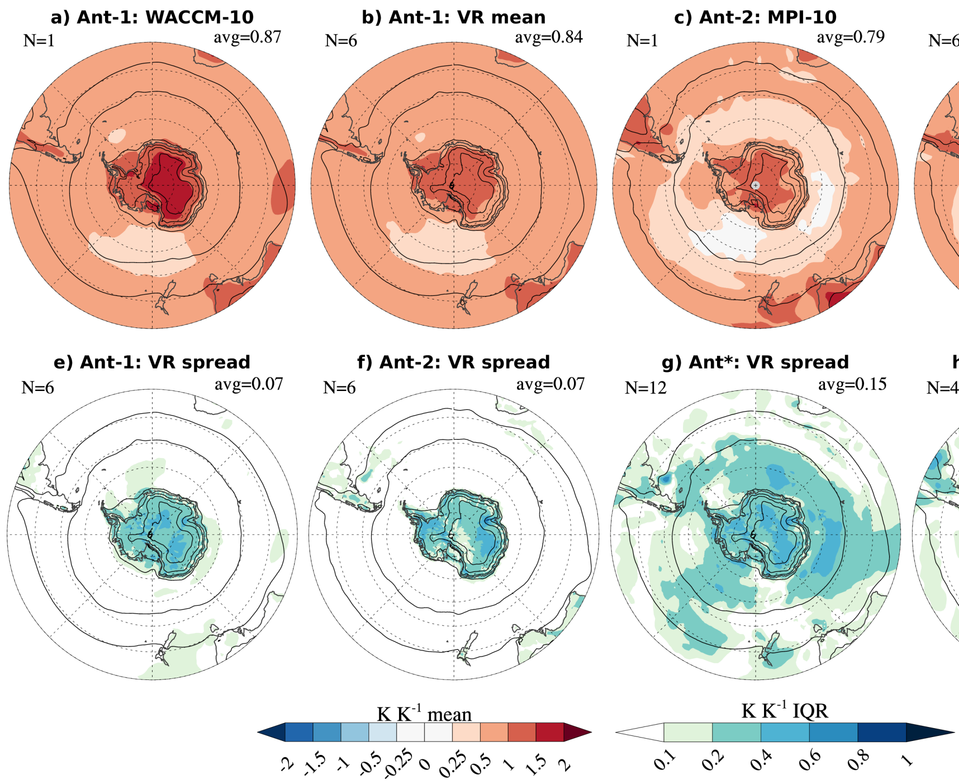

Figure 8. Future changes in near-surface temperature during DJFM for the Ant-1 storyline model (WACCM-10; a), the Ant-1 VR-model mean (CESM/ICON/MPAS-UU/RU; b), the Ant-2 storyline model (MPI-10; c), and the Ant-2 VR-model mean (CESM/ICON/MPAS-UU/RU; d). Also shown is the IQR (spread) for the Ant-1 (e), Ant-2 (f), and for the combined Ant-1 and Ant-2 (g) VR-model responses, and of the combined storyline-model responses for both time periods (WACCM-10/30 and MPI-10/30; h). Future responses are defined in Table S3. Panel titles, color bars, and normalization is as in Fig. 3. Units are K K^{-1}.

Hence, we find that the Antarctic storyline models and VR models generally reproduce the W24 storyline results for DJFM near-surface temperature. There is, however, a less clear distinction between the within- and across-storyline correlation coefficients in the Antarctic storyline experiments (Fig. S5) than in the Arctic experiments (Fig. 5), partly because the across-storyline correlation coefficients are generally higher. This is consistent with the main differences between Ant-1 and Ant-2 occurring in the 50–90°S latitude band, whereas the northernmost parts of the domain are more comparable and therefore more highly correlated (Fig. 8a–d and S4c–d).

For precipitation, W24 (their Fig. 8) found somewhat enhanced precipitation surrounding Antarctica in Ant-2 and enhanced drying further north, upstream of the southern tip of South America, southwest of Africa, and south-southwest of Australia. These features are only partly captured in the storyline models, where the main difference between Ant-1 and Ant-2 is patches of enhanced drying in the 40–60° band (Fig. S4e–h), albeit in somewhat different regions compared to in W24. Furthermore, the VR-model spread generally exceeds the storyline-model spread in this latitude band (Fig. S6f).

https://doi.org/10.5194/egusphere-2026-5525
Preprint. Discussion started: 23 September 2026

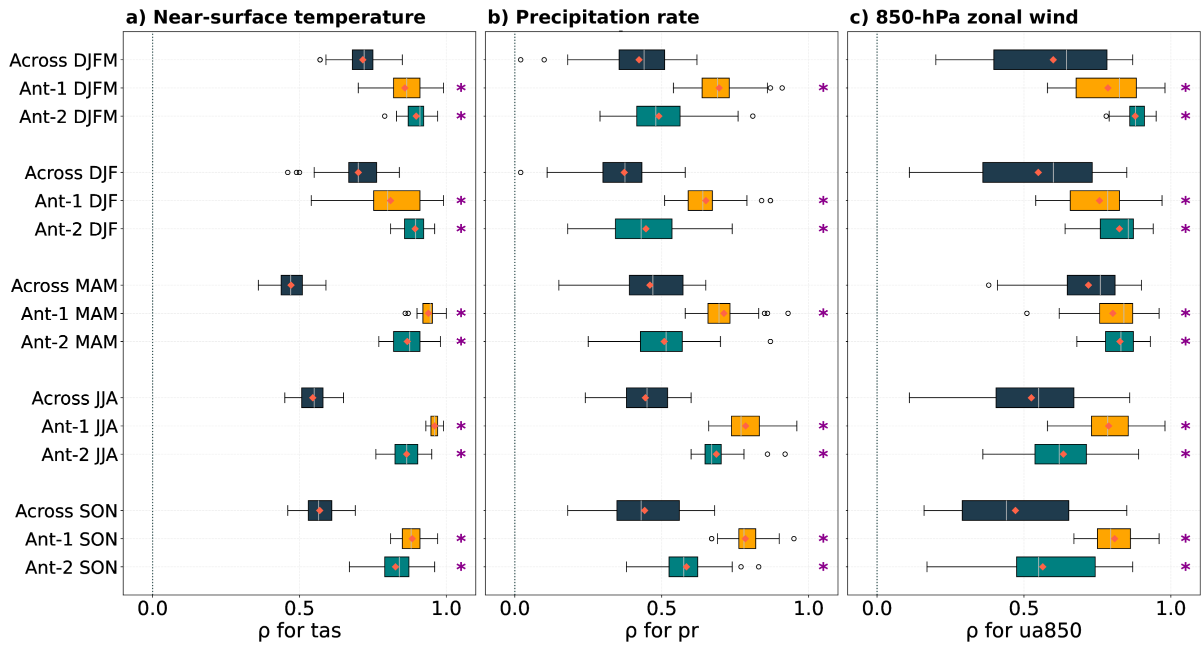

Figure 9. Seasonal distributions of pattern correlation coefficients (ρ) for future changes in the Antarctic storyline-model and VR-model experiments (Ant-1/Ant-2 WACCM/MPI-10/30 and Ant-1/Ant-2 CESM/ICON/MPAS-UU/RU; Table S3) for near-surface temperature (tas; a), total precipitation rate (pr; b), and 850-hPa zonal wind (ua850; c). Distributions are shown for DJFM, DJF, MAM, JJA, and SON for the across-storyline coefficients (dark gray), Ant-1 (yellow), and Ant-2 (teal) coefficients. The distributions, box and whiskers, and magenta asterisks are defined as in Fig. 6, only for the Antarctic storyline experiments. The correlation coefficients are computed for latitudes $\geq 30°$S and cosine weighted. Units are dimensionless.

Our results are more consistent with W24 (their Fig. 6) for 850-hPa zonal wind. The Ant-2 storyline model MPI has a more pronounced poleward shift in the jet than the Ant-1 storyline model WACCM for both periods (Fig. S4i–l). The VR models also reflect this, however, the Ant-1 VR-model-mean response is more zonally symmetric than WACCM (Fig. S7a–b) and the Ant-2 VR-model-mean response has a stronger intensification on the poleward side than MPI (Fig. S7c–d). This results in somewhat weaker contrasts between Ant-1 and Ant-2 in the VR models compared to the storyline models, with the combined storyline-model spread generally exceeding the combined VR-model spread Fig. S7g–h and S6k).

6.2 Separability of Antarctic storyline experiments

Even though the Antarctic storyline experiments appear to be less distinct than the Arctic ones based on the correlation matrix for DJFM near-surface temperature, the Ant-1 and Ant-2 within-storyline distributions are still significantly different from the across-storyline distribution, and thus separable (Fig. 9a). In fact, the Antarctic storylines are separable for all three variables and all seasons, with the exception of precipitation, where Ant-2 is not separable during DJFM and MAM (Fig. 9).

https://doi.org/10.5194/egusphere-2026-5525
Preprint. Discussion started: 23 September 2026

We find the largest separation between the across- and within-storyline distributions for near-surface temperature (Fig. 9a), where the IQR of the across-storyline distribution is positioned entirely below those of Ant-1 and Ant-2, except during DJF when it overlaps somewhat with the Ant-1 IQR. Interestingly, the across-storyline and the Ant-1 and Ant-2 distributions differ more outside the summer season, with the biggest separation occurring in MAM. The Ant-2 distributions are more similar across seasons than Ant-1, which tends to have more pronounced spread during summer (DJF and DJFM).

The precipitation responses are more weakly correlated than the temperature responses, as for the Arctic storylines (Fig. 6b and 9b). Nevertheless, Ant-1 is separable during all seasons and Ant-2 during DJF, JJA, and SON. The largest difference between the across- and within-storyline distributions occur during JJA, potentially tied to winter precipitation having a relatively larger contribution from large-scale precipitation.

For 850-hPa zonal wind, the within-storyline distributions are consistently more highly correlated for the Antarctic storyline experiments compared to the Arctic ones (Fig. 6c and 9c). Ant-1 and Ant-2 are separable for all seasons, and there are no anti-correlated values, like for the Arctic. The separation between the across- and within-storyline distributions is largest during during JJA and SON for Ant-1, and during DJFM and DJF for Ant-2.

While both the Antarctic and Arctic storyline experiments are separable during all seasons for near-surface temperature, the difference between the across- and within-storyline distributions is generally larger for the Antarctic. Furthermore, the Antarctic storyline experiments are more separable for 850-hPa zonal wind. This is likely tied to ocean covering a larger fraction of the surface in the SH, resulting in a relatively larger influence of the prescribed SSTs and SICs. The low-level forcing is closely linked to the sea-ice loss predictor, which exerts a strong influence in the Southern Ocean (Fig. 2).

6.3 Antarctic summary metrics

As for the Arctic, we analyze summary metrics for the influence of the storyline, VR model, and resolution, and for the forcing-model contrast (section 4 and 5.3). We consider the same nine variables as in the Arctic: near-surface, 850-hPa temperature, and 250-hPa temperature, near-surface wind speed, 850-hPa zonal wind, sea level pressure, precipitation, cloud cover, and near-surface humidity (Fig. 10). Consistent with the Arctic results, the resolution generally exerts the weakest influence, but is nevertheless more important for precipitation and clouds, and to some extent for the winds and sea level pressure, than for temperature and near-surface humidity. Interestingly, the influence of resolution on winds and sea level pressure appears somewhat weaker than in the Arctic results (comparing Fig. 7d–f and 10d–f).

The mean storyline influence exceeds the VR-model influence for every season and variable except for 250-hPa temperature and cloud cover (Fig. 10), indicating a more widespread dominance of the storyline influence than in the Arctic. The difference is particularly large for the lower-tropospheric temperature fields and for precipitation (Fig. 10a–b and g), suggesting that contrasting SST and SIC forcings play a larger role in shaping the Antarctic responses. The near-surface temperature, and to a lesser extent the wind and sea level pressure fields, exhibit a stronger storyline influence outside the summer season (Fig. 10a and d–f). For near-surface temperature, the storyline influence closely follows the forcing-model contrast. This shows that while the storylines were designed for summer (DJFM), the storyline-model and the VR-model experiments are actually more distinct for the other seasons for this variable, in line with Fig. 9a.

https://doi.org/10.5194/egusphere-2026-5525
Preprint. Discussion started: 23 September 2026

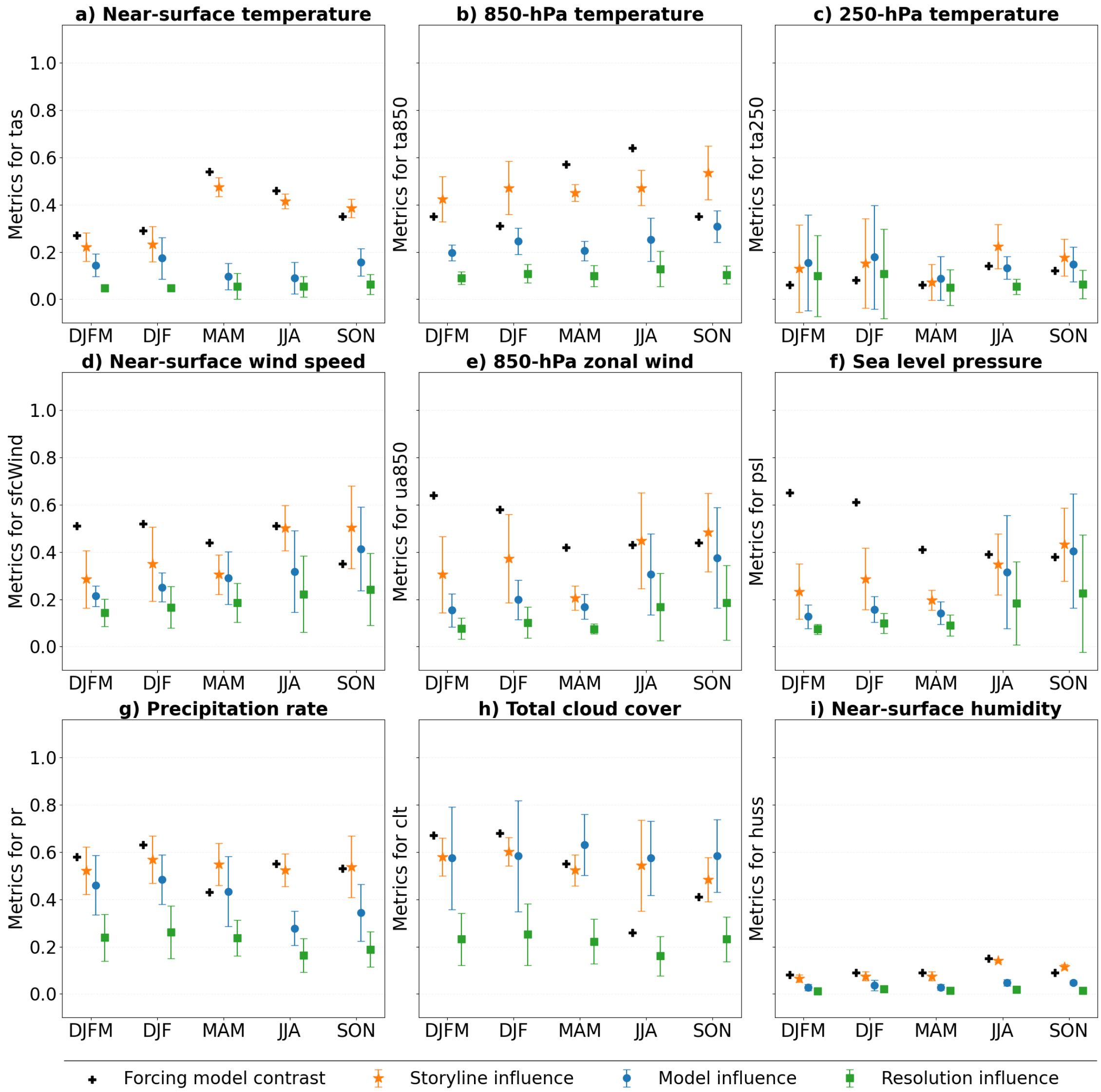

Figure 10. Metrics for the Antarctic storyline-model and VR-model experiments for the influence of the storyline (equation 1 and 2; orange stars), VR model (equation 1 and 3; blue dots), resolution (equation 1 and 4; green squares), and for the forcing-model contrast (equation 1 and 6; black plus signs) for near-surface, 850-hPa, and 250-hPa temperature (tas, ta850, ta250; a–c), near-surface wind speed (sfcWind; d), 850-hPa zonal wind (ua850; e), sea level pressure (psl; f), total precipitation rate (pr; g), total cloud cover (clt; h), and near-surface specific humidity (huss; i) for DJFM, DJF, MAM, JJA, and SON. Markers and bars are as in Fig. 7. The correlation coefficients the metrics are based on are computed for latitudes $\geq 30^{\circ}$S and cosine weighted. Units are dimensionless.

The VR-model influence typically falls somewhere between the influence of the storyline and the resolution, as for the Arctic (Fig. 7 and 10). The VR-model influence is stronger for precipitation and clouds (Fig. 10g–h) than for the other variables,

https://doi.org/10.5194/egusphere-2026-5525
Preprint. Discussion started: 23 September 2026

consistent with the Arctic results. The choice of model exerts a weaker influence on 850-hPa zonal wind than in the Arctic, similar to the resolution influence. The relatively weaker metrics for zonal wind is in line with the future changes in this field being more robust in the SH compared to the NH. This is also reflected in the forcing-model contrast.

The storyline influence closely follows the forcing-model contrast for near-surface temperature and humidity (Fig. 10a and i), indicating that differences between the storyline simulations largely reflect differences already present in the forcing models. This behavior is consistent with the strong influence of the prescribed SST and SIC forcing on Antarctic climate responses over the largely ocean-covered SH.

Near-surface humidity stands out with small values for all metrics and seasons, indicating that the climate change pattern is robust across storylines, VR models, resolutions, and forcing models. Precipitation and clouds appear to be the least robust fields considered here, with consistently relatively large values for all metrics across seasons. Overall, thermodynamic variables are primarily controlled by the imposed storyline forcing, whereas precipitation, cloud cover, and circulation-related variables show a larger sensitivity to model choice and, to a lesser extent, resolution.

7 Summary and discussion

We further explore storylines of Arctic and Antarctic climate change from L24 and W24 (Levine et al., 2024; Williams et al., 2024) using three VR (variable-resolution) models: CESM, ICON, and MPAS. The Arctic storylines represent *weak* AA and *strong* Barents-Kara Sea warming (Arc-1) and *strong* AA and *weak* Barents-Kara-Sea warming (Arc-2) during the extended boreal summer season MJJASO (L24). The Antarctic storylines represent *high* sea-ice loss and *early* vortex breakdown (Ant-1) and *low* sea-ice loss and *late* vortex breakdown (Ant-2) during the extended austral summer season DJFM (W24).

We implement the storyline framework in our VR models by forcing them with daily SSTs and SICs from CMIP6 models that were found by Graff et al. (2026b) and W24 to be representative of the Arctic and Antarctic storylines (the storyline models): CNRM (Arc-1), NorESM (Arc-2), WACCM (Ant-1), and MPI (Ant-2). For each storyline, we conducted a multi-model set of AMIP-style polar refined and unrefined experiments for the future (2090–2099) and unrefined baseline experiments for the recent past (2005–2014), forced with fields from the storyline models' respective CMIP6 historical and SSP5-8.5 experiments. This constitutes the first storyline-based multi-model experiment set with polar refinement.

Based on these experiments, we assess the extent to which using lower-boundary forcing from storyline models representative of contrasting future states result in distinct (separable) future responses for three target variables from L24 and W24: near-surface temperature, total precipitation rate, and 850-hPa zonal wind. To this end, we compute the pattern correlation coefficients across the full set of future responses for each storyline pair (Arc-1 and Arc-2 or Ant-1 and Ant-2), using the storyline-model and unrefined and refined VR-model experiments and evaluate whether the within-storyline coefficients (e.g., Arc-1 versus Arc-1 and Arc-2 versus Arc-2) are significantly different from the across-storyline coefficients (e.g., Arc-1 versus Arc-2). We focus on the mid- and high latitudes for consistency with L24 and W24.

We find the Arctic storyline experiments to be separable for near-surface temperature during all seasons whereas results are more mixed for precipitation and 850-hPa zonal wind. This can potentially be linked to both storyline predictors relating to

https://doi.org/10.5194/egusphere-2026-5525
Preprint. Discussion started: 23 September 2026

low-level Arctic temperature, namely Barents–Kara-Sea SST and pan-Arctic 850-hPa temperature (L24). Furthermore, near-surface temperature is more effectively constrained by the prescribed SSTs than precipitation and 850-hPa zonal wind which are closely tied to the atmospheric circulation and synoptic dynamics and therefore exhibit greater internal variability, consistent with previous work (e.g. Deser et al., 2012a, b, 2014).

The Antarctic storyline experiments are, on the other hand, separable for all three variables except for DJF and MAM precipitation in Ant-2. The distinction between the Arctic and Antarctic storyline experiments is particularly clear for 850-hPa zonal wind, where the Antarctic future responses are more highly correlated and the experiments are separable in more cases. This is likely linked to the much larger ocean fraction in the SH, which renders the SST and SIC forcings more influential.

We also evaluate the extent to which the storyline models and VR models capture the details of the results from L24 and W24 by comparing the regional future responses. For the Antarctic storylines, we find the storyline-model and VR-model experiments to agree well with results from W24 for near-surface temperature and 850-hPa zonal wind, but to a lesser extent for precipitation. For the Arctic, we only find agreement with L24 for near-surface temperature. Nevertheless, the VR-model storyline experiments remain separable in a broader range of cases, showing that the storyline framework applied here can be more generally used to produce contrasting future responses even when the detailed future responses differ from the results in W24 and L24. This is a valuable objective in its own right for applications like Polar CORDEX (Gilbert et al., 2026; Mooney et al., in prep; Mottram et al., 2026).

To quantify the relative importance of the storyline, VR model, resolution, and forcing model, we introduced four summary metrics based the pattern correlations and consider results for a broader range of fields for the mid- and high-latitudes. The resolution influence is generally the weakest factor. Nevertheless, it becomes more important for precipitation and cloud cover, and additionally for winds and sea level pressure in the Arctic experiments. This stronger sensitivity of precipitation- and circulation-related variables to model resolution is consistent with Graff et al. (2026a), who found larger resolution-dependent changes for these fields than for near-surface temperature for the polar regions (their Fig. 16 and S24).

A marked difference emerges between the Arctic and Antarctic storyline experiments. In the Antarctic experiments, the storyline influence dominates for most variables, whereas in the Arctic experiments it is primarily pronounced for near-surface temperature, 850-hPa temperature, and near-surface specific humidity. Given the model set-up, the storyline influence arises from the SST and SIC forcing fields while VR-model influence mainly stems from the atmosphere and land components. The stronger storyline influence in the Antarctic therefore suggests a stronger influence of the prescribed SST and SIC forcing on Antarctic climate-change patterns, consistent with the predominantly ocean-covered SH. In contrast, precipitation, cloud cover, and several circulation-related variables exhibit a stronger dependence on the choice of VR model, indicating a greater sensitivity to model formulation and physical parameterizations.

Our results suggest that for the resolutions explored here, the prescribed SST and SIC forcing and the model used can exert a greater influence on the simulated mid- and high-latitude future response than polar refinement, particularly for low-level thermodynamic fields like near-surface and 850-hPa temperature. Similarly, Mishra et al. (2023) found inter-model differences to tend to exceed inter-resolution differences for the Mediterranean region in experiments from the high-resolution model intercomparison project (HighResMIP; Haarsma et al., 2016). The relatively large impact of the SST and SIC forcing found here is consistent with these fields being derived from CMIP6 models that were selected to represent contrasting future changes, as AMIP-style experiments are known to exhibit sensitivity to changes in the prescribed SST and SIC fields (e.g., Graff and LaCasce, 2012; Smith et al., 2022; Yu et al., 2024). The contrasting behavior of different variables suggests that the dominant source of uncertainty depends on the physical processes involved: thermodynamic variables are largely constrained by the prescribed SST and SIC forcing, whereas precipitation, cloud cover, and circulation-related variables remain more sensitive to atmospheric model formulation. This result can guide the design and interpretation of future storyline-based experiments by identifying the most relevant sources of uncertainty.

While polar refinement tends to have a comparatively weaker influence on the large-scale climate-change patterns explored here than the other influence factors, this should not be interpreted as indicating that high spatial resolution is generally of minor importance for climate projections. Our analysis specifically focuses on large-scale climate-change patterns and is based on data regridded to the coarsest model resolution. This, combined with the lack of refined baseline simulations and the fact that the finest resolution does not cover the entire region of interest, limits our ability to assess high-resolution future responses on a fine grid. Refinement effects occurring at smaller spatial scales are therefore not fully captured by our metrics. Such effects may become more important when focusing on local climate responses, extremes, or impact-relevant processes, for which resolving fine-scale features can be crucial. An indication of such scale-dependent effects is provided by precipitation: restricting the summary metrics to the polar regions, where the highest model resolution is applied, generally reveals a stronger resolution influence (Fig. S8) than for the full domain (Fig. 7g and 10g).

Our results are also limited by the relatively short experiment length (10 years). Longer integration periods or multiple ensemble members would be desirable to further assess the robustness of our results, however, this was not within the scope or resources available for this study. Future work should aim to sample more years or realizations per experiment.

Performing refined recent-past experiments for all three models was not permissible due to limited computing and storage resources, however, the relatively lower resolution used for CESM allowed us to carry them out for that model. We find the CESM-RU responses to generally be highly correlated with the RR (future dual-polar refined−recent-past dual-polar refined) responses, particularly for Ant-1 (Fig. S9). However, the correlation values are notably weaker in some cases, including 850-hPa zonal wind during MAM and SON for Arc-1 and 250-hPa temperature during MAM for Arc-2 and DJFM/DJF for Ant-2 (Fig. S9a, b, and d). Further exploring these differences presents an interesting avenue for future research.

To optimize comparability between the Arctic and Antarctic results, we opted for a harmonized time period for the recent past (2005–2014). This time period however differs from the mid-Century period used in W24. We find that for the time period used here, the storyline models W24 selected predominantly reflect the contrasting sea-ice loss between Ant-1 and Ant-2, while the timing of the SPV breakdown is relatively similar. This highlights the sensitivity of the Antarctic storylines and the storyline-model selection to the historical time period used.

This work focuses on the future response patterns, however, changes in the amplitude of the response are not assessed. This aspect of the future change signal is currently being investigated in a comprehensive set of ICON experiments, including the ones used here, in ongoing work (Köhler et al., in prep.). The ICON model is unique in its ability to be configured both as a global VR model and as a regional climate model (RCM). Köhler et al. (in prep.) will consider the ICON VR-model

https://doi.org/10.5194/egusphere-2026-5525
Preprint. Discussion started: 23 September 2026

experiments presented here context of complementary RCM runs forced with boundary conditions from the same storyline models (Mottram et al., 2026), enabling an additional assessment of the downscaling method.

Data availability. The VR-model data is in the process of being deposited into archives that are freely available to everyone. The CMIP6 data (section 3.4 and Table S1) is freely available through the Earth System Grid Federation (ESGF) nodes (https://esgf.github.io/nodes.html).

Author contributions. LSG coordinated the paper. PAM secured the primary funding for this work and led the overarching project in which this study was conducted. DH and LSG led the work package underpinning this study, coordinated scientific activities throughout the project, and coordinated the development of the experimental protocol with input from all authors. RRW carried out the CESM experiments, RK the ICON experiments, and XL the MPAS experiments. RSW derived and analyzed the Antarctic SST and SIC storylines (section 3.2). LSG and RK conceptualized and performed the analysis in section 5–6 with input from all authors, and RK designed the summary metrics. LSG wrote the first draft together with RK (section 1, 3.3, 4, 6.3, and 7), RSW (section 2 and 3) and XL (section 2 and 3.3) and RRW (section 3.3) with contributions from all authors. All authors reviewed and commented on the manuscript.

Competing interests. We declare that we have no competing interests.

Acknowledgements. All authors were supported by the EU/H2020 project PolarRES (grant number 101003590). In addition, LSG was supported by the Research Council of Norway project BASIC (project number 325440) and INES2 (project number 270061) and DH by the German Research Transregional Collaborative Research Center (TR 172) (AC)^3 (project id 268020496) and the German Federal Ministry of Research, Technology and Space project "TurbO-Arctic" (01LK2317A) under the "WarmWorld" program. High-performance and storage resources were provided by the Computational and Information Systems Laboratory (CISL) at NSF-NCAR (https://doi.org/10.5065/D6RX99HX) for the CESM runs, the Alfred Wegener Institute (AWI) high-performance computing facility Albedo for the ICON runs, and by Sigma2, the National Infrastructure for High-Performance Computing and Data Storage in Norway, for the MPAS runs (projects NN8002K, NS8002K, NS8502K). We also acknowledge Sigma2 for providing resources for joint data analysis and sharing of the VR model and CMIP6 data (projects NS8402K, NS9034K, and NS9560K). We acknowledge the World Climate Research Programme for coordinating and promoting CMIP6 through its Working Group on Coupled Modelling, the CMIP6 modeling groups for producing the model output and making it available, the ESGF for providing access, and the various funding agencies who support CMIP6 and ESGF. We acknowledge Alexey Yu. Karpechko for valuable comments and suggestions on multiple versions of the manuscript.

References

Bader, D. C., Leung, R., Taylor, M., and McCoy, R. B.: E3SM-Project E3SM1.1ECA model output prepared for CMIP6 CMIP historical, https://doi.org/10.22033/ESGF/CMIP6.11486, 2020a.

Bader, D. C., Leung, R., Taylor, M., and McCoy, R. B.: E3SM-Project E3SM1.1 model output prepared for CMIP6 ScenarioMIP ssp585, https://doi.org/10.22033/ESGF/CMIP6.15179, 2020b.

Banwell, A. F., Willis, I. C., Macdonald, G. J., Goodsell, B., and MacAyeal, D. R.: Direct measurements of ice-shelf flexure caused by surface meltwater ponding and drainage, Nature Communications, 10, https://doi.org/10.1038/s41467-019-08522-5, 2019.

Bentsen, M., Oliviè, D. J. L., Seland, Ø., Toniazzo, T., Gjermundsen, A., Graff, L. S., Debernard, J. B., Gupta, A. K., He, Y., Kirkevåg, A., Schwinger, J., Tjiputra, J., Aas, K. S., Bethke, I., Fan, Y., Griesfeller, J., Grini, A., Guo, C., Ilicak, M., Karset, I. H. H., Landgren, O. A., Liakka, J., Moseid, K. O., Nummelin, A., Spensberger, C., Tang, H., Zhang, Z., Heinze, C., Iversen, T., and Schulz, M.: NCC NorESM2-MM model output prepared for CMIP6 CMIP historical, https://doi.org/10.22033/ESGF/CMIP6.8040, 2019a.

Bentsen, M., Oliviè, D. J. L., Seland, Ø., Toniazzo, T., Gjermundsen, A., Graff, L. S., Debernard, J. B., Gupta, A. K., He, Y., Kirkevåg, A., Schwinger, J., Tjiputra, J., Aas, K. S., Bethke, I., Fan, Y., Griesfeller, J., Grini, A., Guo, C., Ilicak, M., Karset, I. H. H., Landgren, O. A., Liakka, J., Moseid, K. O., Nummelin, A., Spensberger, C., Tang, H., Zhang, Z., Heinze, C., Iversen, T., and Schulz, M.: NCC NorESM2-MM model output prepared for CMIP6 ScenarioMIP ssp585, https://doi.org/10.22033/ESGF/CMIP6.8321, 2019b.

Boucher, O., Denvil, S., Levavasseur, G., Cozic, A., Caubel, A., Foujols, M.-A., Meurdesoif, Y., Cadule, P., Devilliers, M., Ghattas, J., Lebas, N., Lurton, T., Mellul, L., Musat, I., Mignot, J., and Cheruy, F.: IPSL IPSL-CM6A-LR model output prepared for CMIP6 CMIP historical, https://doi.org/10.22033/ESGF/CMIP6.5195, 2018.

Boucher, O., Denvil, S., Levavasseur, G., Cozic, A., Caubel, A., Foujols, M.-A., Meurdesoif, Y., Cadule, P., Devilliers, M., Dupont, E., and Lurton, T.: IPSL IPSL-CM6A-LR model output prepared for CMIP6 ScenarioMIP ssp585, https://doi.org/10.22033/ESGF/CMIP6.5271, 2019.

Cao, J.: NUIST NESMv3 model output prepared for CMIP6 ScenarioMIP ssp585, https://doi.org/10.22033/ESGF/CMIP6.8790, 2019.

Cao, J. and Wang, B.: NUIST NESMv3 model output prepared for CMIP6 CMIP historical, https://doi.org/10.22033/ESGF/CMIP6.8769, 2019.

Chai, Z.: CAS CAS-ESM1.0 model output prepared for CMIP6 CMIP historical, https://doi.org/10.22033/ESGF/CMIP6.3353, 2020.

Cheng, W., Dan, L., Deng, X., Feng, J., Wang, Y., Peng, J., Tian, J., Qi, W., Liu, Z., Zheng, X., Zhou, D., Jiang, S., Zhao, H., and Wang, X.: Global monthly gridded atmospheric carbon dioxide concentrations under the historical and future scenarios, Scientific Data, 9, https://doi.org/10.1038/s41597-022-01196-7, 2022.

Chinese Academy Of Sciences (CAS): CAS CAS-ESM1.0 model output prepared for CMIP6 ScenarioMIP ssp585, https://doi.org/10.22033/ESGF/CMIP6.3501, 2020.

Danabasoglu, G.: NCAR CESM2 model output prepared for CMIP6 CMIP historical, https://doi.org/10.22033/ESGF/CMIP6.7627, 2019a.

Danabasoglu, G.: NCAR CESM2 model output prepared for CMIP6 ScenarioMIP ssp585, https://doi.org/10.22033/ESGF/CMIP6.7768, 2019b.

Danabasoglu, G.: NCAR CESM2-WACCM model output prepared for CMIP6 CMIP historical, https://doi.org/10.22033/ESGF/CMIP6.10071, 2019c.

Danabasoglu, G.: NCAR CESM2-WACCM model output prepared for CMIP6 ScenarioMIP ssp585, https://doi.org/10.22033/ESGF/CMIP6.10115, 2019d.

https://doi.org/10.5194/egusphere-2026-5525
Preprint. Discussion started: 23 September 2026

Danabasoglu, G., Lamarque, J., Bacmeister, J., Bailey, D. A., DuVivier, A. K., Edwards, J., Emmons, L. K., Fasullo, J., Garcia, R., Gettelman, A., Hannay, C., Holland, M. M., Large, W. G., Lauritzen, P. H., Lawrence, D. M., Lenaerts, J. T. M., Lindsay, K., Lipscomb, W. H., Mills, M. J., Neale, R., Oleson, K. W., Otto-Bliesner, B., Phillips, A. S., Sacks, W., Tilmes, S., van Kampenhout, L., Vertenstein, M., Bertini, A., Dennis, J., Deser, C., Fischer, C., Fox-Kemper, B., Kay, J. E., Kinnison, D., Kushner, P. J., Larson, V. E., Long, M. C., Mickelson, S., Moore, J. K., Nienhouse, E., Polvani, L., Rasch, P. J., and Strand, W. G.: The Community Earth System Model Version 2 (CESM2), Journal of Advances in Modeling Earth Systems, 12, https://doi.org/10.1029/2019ms001916, 2020.

Deser, C., Knutti, R., Solomon, S., and Phillips, A. S.: Communication of the role of natural variability in future North American climate, Nature Climate Change, 2, 775–779, https://doi.org/10.1038/nclimate1562, 2012a.

Deser, C., Phillips, A., Bourdette, V., and Teng, H.: Uncertainty in climate change projections: the role of internal variability, Climate Dynamics, 38, 527–546, https://doi.org/10.1007/s00382-010-0977-x, 2012b.

Deser, C., Phillips, A. S., Alexander, M. A., and Smoliak, B. V.: Projecting North American Climate over the Next 50 Years: Uncertainty due to Internal Variability*, Journal of Climate, 27, 2271–2296, https://doi.org/10.1175/jcli-d-13-00451.1, 2014.

Dix, M., Bi, D., Dobrohotoff, P., Fiedler, R., Harman, I., Law, R., Mackallah, C., Marsland, S., O'Farrell, S., Rashid, H., Srbinovsky, J., Sullivan, A., Trenham, C., Vohralik, P., Watterson, I., Williams, G., Woodhouse, M., Bodman, R., Dias, F. B., Domingues, C. M., Hannah, N., Heerdegen, A., Savita, A., Wales, S., Allen, C., Druken, K., Evans, B., Richards, C., Ridzwan, S. M., Roberts, D., Smillie, J., Snow, K., Ward, M., and Yang, R.: CSIRO-ARCCSS ACCESS-CM2 model output prepared for CMIP6 CMIP historical, https://doi.org/10.22033/ESGF/CMIP6.4271, 2019a.

Dix, M., Bi, D., Dobrohotoff, P., Fiedler, R., Harman, I., Law, R., Mackallah, C., Marsland, S., O'Farrell, S., Rashid, H., Srbinovsky, J., Sullivan, A., Trenham, C., Vohralik, P., Watterson, I., Williams, G., Woodhouse, M., Bodman, R., Dias, F. B., Domingues, C. M., Hannah, N., Heerdegen, A., Savita, A., Wales, S., Allen, C., Druken, K., Evans, B., Richards, C., Ridzwan, S. M., Roberts, D., Smillie, J., Snow, K., Ward, M., and Yang, R.: CSIRO-ARCCSS ACCESS-CM2 model output prepared for CMIP6 ScenarioMIP ssp585, https://doi.org/10.22033/ESGF/CMIP6.4332, 2019b.

EC-Earth Consortium (EC-Earth): EC-Earth-Consortium EC-Earth3-Veg model output prepared for CMIP6 CMIP historical, https://doi.org/10.22033/ESGF/CMIP6.4706, 2019a.

EC-Earth Consortium (EC-Earth): EC-Earth-Consortium EC-Earth3-Veg model output prepared for CMIP6 ScenarioMIP ssp585, https://doi.org/10.22033/ESGF/CMIP6.4914, 2019b.

EC-Earth Consortium (EC-Earth): EC-Earth-Consortium EC-Earth3 model output prepared for CMIP6 CMIP historical, https://doi.org/10.22033/ESGF/CMIP6.4700, 2019c.

EC-Earth Consortium (EC-Earth): EC-Earth-Consortium EC-Earth3 model output prepared for CMIP6 ScenarioMIP ssp585, https://doi.org/10.22033/ESGF/CMIP6.4912, 2019d.

EC-Earth Consortium (EC-Earth): EC-Earth-Consortium EC-Earth3-Veg-LR model output prepared for CMIP6 CMIP historical, https://doi.org/10.22033/ESGF/CMIP6.4707, 2020a.

EC-Earth Consortium (EC-Earth): EC-Earth-Consortium EC-Earth3-Veg-LR model output prepared for CMIP6 ScenarioMIP ssp585, https://doi.org/10.22033/ESGF/CMIP6.4915, 2020b.

EC-Earth Consortium (EC-Earth): EC-Earth-Consortium EC-Earth-3-CC model output prepared for CMIP6 CMIP historical, https://doi.org/10.22033/ESGF/CMIP6.4702, 2021a.

EC-Earth Consortium (EC-Earth): EC-Earth-Consortium EC-Earth3-CC model output prepared for CMIP6 ScenarioMIP ssp585, https://doi.org/10.22033/ESGF/CMIP6.15636, 2021b.

https://doi.org/10.5194/egusphere-2026-5525
Preprint. Discussion started: 23 September 2026

Eyring, V., Bony, S., Meehl, G. A., Senior, C. A., Stevens, B., Stouffer, R. J., and Taylor, K. E.: Overview of the Coupled Model Intercomparison Project Phase 6 (CMIP6) experimental design and organization, Geoscientific Model Development, 9, 1937–1958, https://doi.org/10.5194/gmd-9-1937-2016, 2016.

Gettelman, A., Callaghan, P., Larson, V. E., Zarzycki, C. M., Bacmeister, J. T., Lauritzen, P. H., Bogenschutz, P. A., and Neale, R. B.: Regional Climate Simulations With the Community Earth System Model, Journal of Advances in Modeling Earth Systems, 10, 1245–1265, https://doi.org/10.1002/2017ms001227, 2018.

Gettelman, A., Mills, M. J., Kinnison, D. E., Garcia, R. R., Smith, A. K., Marsh, D. R., Tilmes, S., Vitt, F., Bardeen, C. G., McInerny, J., Liu, H., Solomon, S. C., Polvani, L. M., Emmons, L. K., Lamarque, J., Richter, J. H., Glanville, A. S., Bacmeister, J. T., Phillips, A. S., Neale, R. B., Simpson, I. R., DuVivier, A. K., Hodzic, A., and Randel, W. J.: The Whole Atmosphere Community Climate Model Version 6 (WACCM6), Journal of Geophysical Research: Atmospheres, 124, 12 380–12 403, https://doi.org/10.1029/2019jd030943, 2019.

Gilbert, E. and Kittel, C.: Surface Melt and Runoff on Antarctic Ice Shelves at 1.5°C, 2°C, and 4°C of Future Warming, Geophysical Research Letters, 48, https://doi.org/10.1029/2020gl091733, 2021.

Gilbert, E., Pishniak, D., Torres, J. A., Orr, A., Maclennan, M., Wever, N., and Verro, K.: Extreme precipitation associated with atmospheric rivers over West Antarctic ice shelves: insights from kilometre-scale regional climate modelling, The Cryosphere, 19, 597–618, https://doi.org/10.5194/tc-19-597-2025, 2025.

Gilbert, E., Torres-Alavez, J. A., Hofsteenge, M. G., van de Berg, W. J., Boberg, F., Christensen, O. B., van Dalum, C. T., Fettweis, X., Gumber, S., Hansen, N., Kittel, C., Lambin, C., Maure, D., Mottram, R., Olesen, M., Orr, A., Phillips, T., van Tiggelen, M., Verro, K., and Mooney, P. A.: The PolarRES dataset: a state-of-the-art regional climate model ensemble for understanding Antarctic climate, The Cryosphere, 20, 2629–2658, https://doi.org/10.5194/tc-20-2629-2026, 2026.

Good, P.: MOHC HadGEM3-GC31-LL model output prepared for CMIP6 ScenarioMIP ssp585, https://doi.org/10.22033/ESGF/CMIP6.10901, 2020.

Good, P., Sellar, A., Tang, Y., Rumbold, S., Ellis, R., Kelley, D., and Kuhlbrodt, T.: MOHC UKESM1.0-LL model output prepared for CMIP6 ScenarioMIP ssp585, https://doi.org/10.22033/ESGF/CMIP6.6405, 2019.

Graff, L. S. and LaCasce, J. H.: Changes in the Extratropical Storm Tracks in Response to Changes in SST in an AGCM, Journal of Climate, 25, 1854–1870, https://doi.org/10.1175/jcli-d-11-00174.1, 2012.

Graff, L. S., Handorf, D., Köhler, R., Levine, X., Wijngaard, R. R., Marshall, G. J., Karpechko, A. Y., Williams, R. S., and Mooney, P. A.: A multimodel intercomparison study of variable-resolution global models with grid refinement over the Arctic and Antarctic, Quarterly Journal of the Royal Meteorological Society, https://doi.org/10.1002/qj.70192, 2026a.

Graff, L. S., Landgren, O. A., Parding, K. M., Levine, X., Williams, R. S., and Mooney, P. A.: Selecting CMIP6 Models for Future Arctic Storylines Using a Novel Performance Score, Tellus, 78, 1–21, https://doi.org/10.16993/tellusa.4111, 2026b.

Guo, H., John, J. G., Blanton, C., McHugh, C., Nikonov, S., Radhakrishnan, A., Rand, K., Zadeh, N. T., Balaji, V., Durachta, J., Dupuis, C., Menzel, R., Robinson, T., Underwood, S., Vahlenkamp, H., Bushuk, M., Dunne, K. A., Dussin, R., Gauthier, P. P., Ginoux, P., Griffies, S. M., Hallberg, R., Harrison, M., Hurlin, W., Lin, P., Malyshev, S., Naik, V., Paulot, F., Paynter, D. J., Ploshay, J., Reichl, B. G., Schwarzkopf, D. M., Seman, C. J., Shao, A., Silvers, L., Wyman, B., Yan, X., Zeng, Y., Adcroft, A., Dunne, J. P., Held, I. M., Krasting, J. P., Horowitz, L. W., Milly, P., Shevliakova, E., Winton, M., Zhao, M., and Zhang, R.: NOAA-GFDL GFDL-CM4 model output historical, https://doi.org/10.22033/ESGF/CMIP6.8594, 2018a.

Guo, H., John, J. G., Blanton, C., McHugh, C., Nikonov, S., Radhakrishnan, A., Rand, K., Zadeh, N. T., Balaji, V., Durachta, J., Dupuis, C., Menzel, R., Robinson, T., Underwood, S., Vahlenkamp, H., Dunne, K. A., Gauthier, P. P., Ginoux, P., Griffies, S. M., Hallberg, R., Harrison, M., Hurlin, W., Lin, P., Malyshev, S., Naik, V., Paulot, F., Paynter, D. J., Ploshay, J., Schwarzkopf, D. M., Seman, C. J., Shao, A., Silvers, L., Wyman, B., Yan, X., Zeng, Y., Adcroft, A., Dunne, J. P., Held, I. M., Krasting, J. P., Horowitz, L. W., Milly, C., Shevliakova, E., Winton, M., Zhao, M., and Zhang, R.: NOAA-GFDL GFDL-CM4 model output prepared for CMIP6 ScenarioMIP ssp585, https://doi.org/10.22033/ESGF/CMIP6.9268, 2018b.

Haarsma, R. J., Roberts, M. J., Vidale, P. L., Senior, C. A., Bellucci, A., Bao, Q., Chang, P., Corti, S., Fučkar, N. S., Guemas, V., von Hardenberg, J., Hazeleger, W., Kodama, C., Koenigk, T., Leung, L. R., Lu, J., Luo, J.-J., Mao, J., Mizielinski, M. S., Mizuta, R., Nobre, P., Satoh, M., Scoccimarro, E., Semmler, T., Small, J., and von Storch, J.-S.: High Resolution Model Intercomparison Project (HighResMIP v1.0) for CMIP6, Geoscientific Model Development, 9, 4185–4208, https://doi.org/10.5194/gmd-9-4185-2016, 2016.

Hawkins, E. and Sutton, R.: The Potential to Narrow Uncertainty in Regional Climate Predictions, Bulletin of the American Meteorological Society, 90, 1095–1108, https://doi.org/10.1175/2009bams2607.1, 2009.

Hegglin, M., Kinnison, D., Lamarque, J.-F., and Plummer, D.: CCMI ozone in support of CMIP6 - version 1.0, https://doi.org/10.22033/ESGF/INPUT4MIPS.1115, 2016.

Herrington, A. R., Lauritzen, P. H., Lofverstrom, M., Lipscomb, W. H., Gettelman, A., and Taylor, M. A.: Impact of Grids and Dynamical Cores in CESM2.2 on the Surface Mass Balance of the Greenland Ice Sheet, Journal of Advances in Modeling Earth Systems, 14, https://doi.org/10.1029/2022ms003192, 2022.

Hersbach, H., Bell, B., Berrisford, P., Hirahara, S., Horányi, A., Muñoz-Sabater, J., Nicolas, J., Peubey, C., Radu, R., Schepers, D., Simmons, A., Soci, C., Abdalla, S., Abellan, X., Balsamo, G., Bechtold, P., Biavati, G., Bidlot, J., Bonavita, M., De Chiara, G., Dahlgren, P., Dee, D., Diamantakis, M., Dragani, R., Flemming, J., Forbes, R., Fuentes, M., Geer, A., Haimberger, L., Healy, S., Hogan, R. J., Hólm, E., Janisková, M., Keeley, S., Laloyaux, P., Lopez, P., Lupu, C., Radnoti, G., de Rosnay, P., Rozum, I., Vamborg, F., Villaume, S., and Thépaut, J.: The ERA5 global reanalysis, Quarterly Journal of the Royal Meteorological Society, 146, 1999–2049, https://doi.org/10.1002/qj.3803, 2020.

Hoesly, R. M., Smith, S. J., Feng, L., Klimont, Z., Janssens-Maenhout, G., Pitkanen, T., Seibert, J. J., Vu, L., Andres, R. J., Bolt, R. M., Bond, T. C., Dawidowski, L., Kholod, N., Kurokawa, J.-i., Li, M., Liu, L., Lu, Z., Moura, M. C. P., O'Rourke, P. R., and Zhang, Q.: Historical (1750–2014) anthropogenic emissions of reactive gases and aerosols from the Community Emissions Data System (CEDS), Geoscientific Model Development, 11, 369–408, https://doi.org/10.5194/gmd-11-369-2018, 2018.

Huang, W.: THU CIESM model output prepared for CMIP6 CMIP historical, https://doi.org/10.22033/ESGF/CMIP6.8843, 2019.

Huang, W.: THU CIESM model output prepared for CMIP6 ScenarioMIP ssp585, https://doi.org/10.22033/ESGF/CMIP6.8863, 2020.

Jackson, L.: MOHC HadGEM3-GC31-MM model output prepared for CMIP6 ScenarioMIP ssp585, https://doi.org/10.22033/ESGF/CMIP6.10902, 2020.

John, J. G., Blanton, C., McHugh, C., Radhakrishnan, A., Rand, K., Vahlenkamp, H., Wilson, C., Zadeh, N. T., Dunne, J. P., Dussin, R., Horowitz, L. W., Krasting, J. P., Lin, P., Malyshev, S., Naik, V., Ploshay, J., Shevliakova, E., Silvers, L., Stock, C., Winton, M., and Zeng, Y.: NOAA-GFDL GFDL-ESM4 model output prepared for CMIP6 ScenarioMIP ssp585, https://doi.org/10.22033/ESGF/CMIP6.8706, 2018.

Jungclaus, J., Bittner, M., Wieners, K.-H., Wachsmann, F., Schupfner, M., Legutke, S., Giorgetta, M., Reick, C., Gayler, V., Haak, H., de Vrese, P., Raddatz, T., Esch, M., Mauritsen, T., von Storch, J.-S., Behrens, J., Brovkin, V., Claussen, M., Crueger, T., Fast, I., Fiedler, S., Hagemann, S., Hohenegger, C., Jahns, T., Kloster, S., Kinne, S., Lasslop, G., Kornblueh, L., Marotzke, J., Matei, D., Meraner, K., Mikolajewicz, U., Modali, K., Müller, W., Nabel, J., Notz, D., Peters-von Gehlen, K., Pincus, R., Pohlmann, H., Pongratz, J., Rast, S.,

https://doi.org/10.5194/egusphere-2026-5525
Preprint. Discussion started: 23 September 2026

Schmidt, H., Schnur, R., Schulzweida, U., Six, K., Stevens, B., Voigt, A., and Roeckner, E.: MPI-M MPI-ESM1.2-HR model output prepared for CMIP6 CMIP historical, https://doi.org/10.22033/ESGF/CMIP6.6594, 2019.

Keil, P., Mauritsen, T., Jungclaus, J., Hedemann, C., Olonscheck, D., and Ghosh, R.: Multiple drivers of the North Atlantic warming hole, Nature Climate Change, 10, 667–671, https://doi.org/10.1038/s41558-020-0819-8, 2020.

Kim, Y., Noh, Y., Kim, D., Lee, M.-I., Lee, H. J., Kim, S. Y., and Kim, D.: KIOST KIOST-ESM model output prepared for CMIP6 CMIP historical, https://doi.org/10.22033/ESGF/CMIP6.5296, 2019a.

Kim, Y., Noh, Y., Kim, D., Lee, M.-I., Lee, H. J., Kim, S. Y., and Kim, D.: KIOST KIOST-ESM model output prepared for CMIP6 ScenarioMIP ssp585, https://doi.org/10.22033/ESGF/CMIP6.11249, 2019b.

Köhler, R., Matthes, H., Graff, L. S., Zheng, Q., Krishnan, S. R. R., Richter, K., Landwehrs, J., and Handorf, D.: Quantifying structural uncertainty in Arctic climate projections across downscaling approaches within the same model, in prep.

Krasting, J. P., John, J. G., Blanton, C., McHugh, C., Nikonov, S., Radhakrishnan, A., Rand, K., Zadeh, N. T., Balaji, V., Durachta, J., Dupuis, C., Menzel, R., Robinson, T., Underwood, S., Vahlenkamp, H., Dunne, K. A., Gauthier, P. P., Ginoux, P., Griffies, S. M., Hallberg, R., Harrison, M., Hurlin, W., Malyshev, S., Naik, V., Paulot, F., Paynter, D. J., Ploshay, J., Reichl, B. G., Schwarzkopf, D. M., Seman, C. J., Silvers, L., Wyman, B., Zeng, Y., Adcroft, A., Dunne, J. P., Dussin, R., Guo, H., He, J., Held, I. M., Horowitz, L. W., Lin, P., Milly, P., Shevliakova, E., Stock, C., Winton, M., Wittenberg, A. T., Xie, Y., and Zhao, M.: NOAA-GFDL GFDL-ESM4 model output prepared for CMIP6 CMIP historical, https://doi.org/10.22033/ESGF/CMIP6.8597, 2018.

Lai, C.-Y., Kingslake, J., Wearing, M. G., Chen, P.-H. C., Gentine, P., Li, H., Spergel, J. J., and van Wessem, J. M.: Vulnerability of Antarctica's ice shelves to meltwater-driven fracture, Nature, 584, 574–578, https://doi.org/10.1038/s41586-020-2627-8, 2020.

Lauritzen, P. H., Nair, R. D., Herrington, A. R., Callaghan, P., Goldhaber, S., Dennis, J. M., Bacmeister, J. T., Eaton, B. E., Zarzycki, C. M., Taylor, M. A., Ullrich, P. A., Dubos, T., Gettelman, A., Neale, R. B., Dobbins, B., Reed, K. A., Hannay, C., Medeiros, B., Benedict, J. J., and Tribbia, J. J.: NCAR Release of CAM-SE in CESM2.0: A Reformulation of the Spectral Element Dynamical Core in Dry-Mass Vertical Coordinates With Comprehensive Treatment of Condensates and Energy, Journal of Advances in Modeling Earth Systems, 10, 1537–1570, https://doi.org/10.1029/2017ms001257, 2018.

Lawrence, D. M., Fisher, R. A., Koven, C. D., Oleson, K. W., Swenson, S. C., Bonan, G., Collier, N., Ghimire, B., van Kampenhout, L., Kennedy, D., Kluzek, E., Lawrence, P. J., Li, F., Li, H., Lombardozzi, D., Riley, W. J., Sacks, W. J., Shi, M., Vertenstein, M., Wieder, W. R., Xu, C., Ali, A. A., Badger, A. M., Bisht, G., van den Broeke, M., Brunke, M. A., Burns, S. P., Buzan, J., Clark, M., Craig, A., Dahlin, K., Drewniak, B., Fisher, J. B., Flanner, M., Fox, A. M., Gentine, P., Hoffman, F., Keppel-Aleks, G., Knox, R., Kumar, S., Lenaerts, J., Leung, L. R., Lipscomb, W. H., Lu, Y., Pandey, A., Pelletier, J. D., Perket, J., Randerson, J. T., Ricciuto, D. M., Sanderson, B. M., Slater, A., Subin, Z. M., Tang, J., Thomas, R. Q., Val Martin, M., and Zeng, X.: The Community Land Model Version 5: Description of New Features, Benchmarking, and Impact of Forcing Uncertainty, Journal of Advances in Modeling Earth Systems, 11, 4245–4287, https://doi.org/10.1029/2018ms001583, 2019.

Levine, X. J., Williams, R. S., Marshall, G., Orr, A., Seland Graff, L., Handorf, D., Karpechko, A., Köhler, R., Wijngaard, R. R., Johnston, N., Lee, H., Nieradzik, L., and Mooney, P. A.: Storylines of summer Arctic climate change constrained by Barents–Kara seas and Arctic tropospheric warming for climate risk assessment, Earth System Dynamics, 15, 1161–1177, https://doi.org/10.5194/esd-15-1161-2024, 2024.

Liang, Y., Yang, B., Wang, M., Tang, J., Sakaguchi, K., Leung, L. R., and Xu, X.: Multiscale Simulation of Precipitation Over East Asia by Variable Resolution CAM-MPAS, Journal of Advances in Modeling Earth Systems, 13, https://doi.org/10.1029/2021ms002656, 2021.

https://doi.org/10.5194/egusphere-2026-5525
Preprint. Discussion started: 23 September 2026

Liu, W., Fedorov, A. V., Xie, S.-P., and Hu, S.: Climate impacts of a weakened Atlantic Meridional Overturning Circulation in a warming climate, Science Advances, 6, https://doi.org/10.1126/sciadv.aaz4876, 2020.

Loeb, N. A., Crawford, A., Herrington, A., McCrystall, M., Stroeve, J., and Hanesiak, J.: Projections and Physical Drivers of Extreme Precipitation in Greenland & Baffin Bay, Journal of Geophysical Research: Atmospheres, 129, https://doi.org/10.1029/2024jd041375, 2024.

Lovato, T. and Peano, D.: CMCC CMCC-CM2-SR5 model output prepared for CMIP6 ScenarioMIP ssp585, https://doi.org/10.22033/ESGF/CMIP6.3896, 2020a.

Lovato, T. and Peano, D.: CMCC CMCC-CM2-SR5 model output prepared for CMIP6 CMIP historical, https://doi.org/10.22033/ESGF/CMIP6.3825, 2020b.

Lovato, T., Peano, D., and Butenschön, M.: CMCC CMCC-ESM2 model output prepared for CMIP6 ScenarioMIP ssp585, https://doi.org/10.22033/ESGF/CMIP6.13259, 2021a.

Lovato, T., Peano, D., and Butenschön, M.: CMCC CMCC-ESM2 model output prepared for CMIP6 CMIP historical, https://doi.org/10.22033/ESGF/CMIP6.13195, 2021b.

Mauritsen, T., Bader, J., Becker, T., Behrens, J., Bittner, M., Brokopf, R., Brovkin, V., Claussen, M., Crueger, T., Esch, M., Fast, I., Fiedler, S., Fläschner, D., Gayler, V., Giorgetta, M., Goll, D. S., Haak, H., Hagemann, S., Hedemann, C., Hohenegger, C., Ilyina, T., Jahns, T., Jimenéz-de-la-Cuesta, D., Jungclaus, J., Kleinen, T., Kloster, S., Kracher, D., Kinne, S., Kleberg, D., Lasslop, G., Kornblueh, L., Marotzke, J., Matei, D., Meraner, K., Mikolajewicz, U., Modali, K., Möbis, B., Müller, W. A., Nabel, J. E. M. S., Nam, C. C. W., Notz, D., Nyawira, S., Paulsen, H., Peters, K., Pincus, R., Pohlmann, H., Pongratz, J., Popp, M., Raddatz, T. J., Rast, S., Redler, R., Reick, C. H., Rohrschneider, T., Schemann, V., Schmidt, H., Schnur, R., Schulzweida, U., Six, K. D., Stein, L., Stemmler, I., Stevens, B., von Storch, J., Tian, F., Voigt, A., Vrese, P., Wieners, K., Wilkenskjeld, S., Winkler, A., and Roeckner, E.: Developments in the MPI-M Earth System Model version 1.2 (MPI-ESM1.2) and Its Response to Increasing CO2, Journal of Advances in Modeling Earth Systems, 11, 998–1038, https://doi.org/10.1029/2018ms001400, 2019.

Meinshausen, M., Vogel, E., Nauels, A., Lorbacher, K., Meinshausen, N., Etheridge, D. M., Fraser, P. J., Montzka, S. A., Rayner, P. J., Trudinger, C. M., Krummel, P. B., Beyerle, U., Canadell, J. G., Daniel, J. S., Enting, I. G., Law, R. M., Lunder, C. R., O'Doherty, S., Prinn, R. G., Reimann, S., Rubino, M., Velders, G. J. M., Vollmer, M. K., Wang, R. H. J., and Weiss, R.: Historical greenhouse gas concentrations for climate modelling (CMIP6), Geoscientific Model Development, 10, 2057–2116, https://doi.org/10.5194/gmd-10-2057-2017, 2017.

Mindlin, J., Shepherd, T. G., Vera, C. S., Osman, M., Zappa, G., Lee, R. W., and Hodges, K. I.: Storyline description of Southern Hemisphere midlatitude circulation and precipitation response to greenhouse gas forcing, Climate Dynamics, 54, 4399–4421, https://doi.org/10.1007/s00382-020-05234-1, 2020.

Mishra, A. K., Jangir, B., and Strobach, E.: Does Increasing Climate Model Horizontal Resolution Be Beneficial for the Mediterranean Region?: Multimodel Evaluation Framework for High-Resolution Model Intercomparison Project, Journal of Geophysical Research: Atmospheres, 128, https://doi.org/10.1029/2022jd037812, 2023.

Mitchell, D., AchutaRao, K., Allen, M., Bethke, I., Beyerle, U., Ciavarella, A., Forster, P. M., Fuglestvedt, J., Gillett, N., Haustein, K., Ingram, W., Iversen, T., Kharin, V., Klingaman, N., Massey, N., Fischer, E., Schleussner, C.-F., Scinocca, J., Seland, Ø., Shiogama, H., Shuckburgh, E., Sparrow, S., Stone, D., Uhe, P., Wallom, D., Wehner, M., and Zaaboul, R.: Half a degree additional warming, prognosis and projected impacts (HAPPI): background and experimental design, Geoscientific Model Development, 10, 571–583, https://doi.org/10.5194/gmd-10-571-2017, 2017.

https://doi.org/10.5194/egusphere-2026-5525
Preprint. Discussion started: 23 September 2026

Mooney, P. A., Falco, C. D., Samantaray, A. K., van de Berg, W. J., Cassano, J., Gilbert, E., Landwehrs, J., Matthes, H., Mottram, R., Orr, A., Rinke, A., Parker, C. L., Maslowski, W., and Zhang, X.: Pan-Arctic high resolution regional climate model ensemble: Performance of the PolarRES and Arctic CORDEX ensemble, in prep.

Mottram, R., Mooney, P. A., Äijälä, C., van de Berg, W. J., Bezhenar, R., Bhatt, B. C., Boberg, F., Cherblanc, C., Christensen, O. B., Chyhareva, A., van Dalum, C. T., Falco, C. D., Fettweis, X., Gadde, S. N., Gilbert, E., Gumber, S., Haakenstad, H., Hansen, N., Johnston, N. M., Kittel, C., Krakovska, S., Lambin, C., Landwehrs, J., Landgren, O., Lee, H., Levine, X., Matthes, H., Maure, D., Naakka, T., Negrel, J., Nieradzik, L. P., Olesen, M., Orr, A., Phillips, T., Pishniak, D., Rinke, A., Alavez, J. A. T., Uotila, P., Verro, K., Vihma, T., and Williams, R. S.: Experimental Protocol (v1) for High Resolution Regional Climate Model Simulations in the Arctic and Antarctica, Geoscientific Model Development, manuscript submitted for publication, 2026.

NASA Goddard Institute For Space Studies (NASA/GISS): NASA-GISS GISS-E2.1G model output prepared for CMIP6 CMIP historical, https://doi.org/10.22033/ESGF/CMIP6.7127, 2018.

NASA Goddard Institute For Space Studies (NASA/GISS): NASA-GISS GISS-E2.1G model output prepared for CMIP6 ScenarioMIP ssp585, https://doi.org/10.22033/ESGF/CMIP6.7460, 2020.

O'Neill, B. C., Tebaldi, C., van Vuuren, D. P., Eyring, V., Friedlingstein, P., Hurtt, G., Knutti, R., Kriegler, E., Lamarque, J.-F., Lowe, J., Meehl, G. A., Moss, R., Riahi, K., and Sanderson, B. M.: The Scenario Model Intercomparison Project (ScenarioMIP) for CMIP6, Geoscientific Model Development, 9, 3461–3482, https://doi.org/10.5194/gmd-9-3461-2016, 2016.

Ridley, J., Menary, M., Kuhlbrodt, T., Andrews, M., and Andrews, T.: MOHC HadGEM3-GC31-LL model output prepared for CMIP6 CMIP historical, https://doi.org/10.22033/ESGF/CMIP6.6109, 2019a.

Ridley, J., Menary, M., Kuhlbrodt, T., Andrews, M., and Andrews, T.: MOHC HadGEM3-GC31-MM model output prepared for CMIP6 CMIP historical, https://doi.org/10.22033/ESGF/CMIP6.6112, 2019b.

Ringler, T., Thuburn, J., Klemp, J., and Skamarock, W.: A unified approach to energy conservation and potential vorticity dynamics for arbitrarily-structured C-grids, Journal of Computational Physics, 229, 3065–3090, https://doi.org/10.1016/j.jcp.2009.12.007, 2010.

Rong, X.: CAMS CAMS_CSM1.0 model output prepared for CMIP6 CMIP historical, https://doi.org/10.22033/ESGF/CMIP6.9754, 2019a.

Rong, X.: CAMS CAMS-CSM1.0 model output prepared for CMIP6 ScenarioMIP ssp585, https://doi.org/10.22033/ESGF/CMIP6.11052, 2019b.

Scambos, T., Hulbe, C., and Fahnestock, M.: Climate-Induced Ice Shelf Disintegration in the Antarctic Peninsula, pp. 79–92, American Geophysical Union, ISBN 9780875909738, https://doi.org/10.1029/ar079p0079, 2013.

Schupfner, M., Wieners, K.-H., Wachsmann, F., Steger, C., Bittner, M., Jungclaus, J., Früh, B., Pankatz, K., Giorgetta, M., Reick, C., Legutke, S., Esch, M., Gayler, V., Haak, H., de Vrese, P., Raddatz, T., Mauritsen, T., von Storch, J.-S., Behrens, J., Brovkin, V., Claussen, M., Crueger, T., Fast, I., Fiedler, S., Hagemann, S., Hohenegger, C., Jahns, T., Kloster, S., Kinne, S., Lasslop, G., Kornblueh, L., Marotzke, J., Matei, D., Meraner, K., Mikolajewicz, U., Modali, K., Müller, W., Nabel, J., Notz, D., Peters-von Gehlen, K., Pincus, R., Pohlmann, H., Pongratz, J., Rast, S., Schmidt, H., Schnur, R., Schulzweida, U., Six, K., Stevens, B., Voigt, A., and Roeckner, E.: DKRZ MPI-ESM1.2-HR model output prepared for CMIP6 ScenarioMIP ssp585, https://doi.org/10.22033/ESGF/CMIP6.4403, 2019.

Seferian, R.: CNRM-CERFACS CNRM-ESM2-1 model output prepared for CMIP6 CMIP historical, https://doi.org/10.22033/ESGF/CMIP6.4068, 2018a.

Seferian, R.: CNRM-CERFACS CNRM-ESM2-1 model output prepared for CMIP6 CMIP historical, https://doi.org/10.22033/ESGF/CMIP6.4068, 2018b.

Séférian, R., Nabat, P., Michou, M., Saint-Martin, D., Voldoire, A., Colin, J., Decharme, B., Delire, C., Berthet, S., Chevallier, M., Sénési, S., Franchisteguy, L., Vial, J., Mallet, M., Joetzjer, E., Geoffroy, O., Guérémy, J., Moine, M., Msadek, R., Ribes, A., Rocher, M., Roehrig, R., Salas-y-Mélia, D., Sanchez, E., Terray, L., Valcke, S., Waldman, R., Aumont, O., Bopp, L., Deshayes, J., Éthé, C., and Madec, G.: Evaluation of CNRM Earth System Model, CNRM-ESM2-1: Role of Earth System Processes in Present-Day and Future Climate, Journal of Advances in Modeling Earth Systems, 11, 4182–4227, https://doi.org/10.1029/2019ms001791, 2019.

Seland, Ø., Bentsen, M., Olivié, D., Toniazzo, T., Gjermundsen, A., Graff, L. S., Debernard, J. B., Gupta, A. K., He, Y.-C., Kirkevåg, A., Schwinger, J., Tjiputra, J., Aas, K. S., Bethke, I., Fan, Y., Griesfeller, J., Grini, A., Guo, C., Ilicak, M., Karset, I. H. H., Landgren, O., Liakka, J., Moseid, K. O., Nummelin, A., Spensberger, C., Tang, H., Zhang, Z., Heinze, C., Iversen, T., and Schulz, M.: Overview of the Norwegian Earth System Model (NorESM2) and key climate response of CMIP6 DECK, historical, and scenario simulations, Geoscientific Model Development, 13, 6165–6200, https://doi.org/10.5194/gmd-13-6165-2020, 2020.

Shepherd, T. G.: Atmospheric circulation as a source of uncertainty in climate change projections, Nature Geoscience, 7, 703–708, https://doi.org/10.1038/ngeo2253, 2014.

Skamarock, W. C., Klemp, J. B., Duda, M. G., Fowler, L. D., Park, S.-H., and Ringler, T. D.: A Multiscale Nonhydrostatic Atmospheric Model Using Centroidal Voronoi Tesselations and C-Grid Staggering, Monthly Weather Review, 140, 3090–3105, https://doi.org/10.1175/mwr-d-11-00215.1, 2012.

Smith, D. M., Eade, R., Andrews, M. B., Ayres, H., Clark, A., Chripko, S., Deser, C., Dunstone, N. J., García-Serrano, J., Gastineau, G., Graff, L. S., Hardiman, S. C., He, B., Hermanson, L., Jung, T., Knight, J., Levine, X., Magnusdottir, G., Manzini, E., Matei, D., Mori, M., Msadek, R., Ortega, P., Peings, Y., Scaife, A. A., Screen, J. A., Seabrook, M., Semmler, T., Sigmond, M., Streffing, J., Sun, L., and Walsh, A.: Robust but weak winter atmospheric circulation response to future Arctic sea ice loss, Nature Communications, 13, https://doi.org/10.1038/s41467-022-28283-y, 2022.

Song, Z., Qiao, F., Bao, Y., Shu, Q., Song, Y., and Yang, X.: FIO-QLNM FIO-ESM2.0 model output prepared for CMIP6 CMIP historical, https://doi.org/10.22033/ESGF/CMIP6.9199, 2019a.

Song, Z., Qiao, F., Bao, Y., Shu, Q., Song, Y., and Yang, X.: FIO-QLNM FIO-ESM2.0 model output prepared for CMIP6 ScenarioMIP ssp585, https://doi.org/10.22033/ESGF/CMIP6.9214, 2019b.

Sun, L., Wills, R. C. J., Deser, C., Herrington, A., Simpson, I. R., and Gervais, M.: Increased Model Resolution Amplifies Boreal Winter Arctic Precipitation and Atmospheric Circulation Response to Sea Ice Loss, Journal of Climate, 39, 2039–2060, https://doi.org/10.1175/jcli-d-25-0260.1, 2026.

Tang, Y., Rumbold, S., Ellis, R., Kelley, D., Mulcahy, J., Sellar, A., Walton, J., and Jones, C.: MOHC UKESM1.0-LL model output prepared for CMIP6 CMIP historical, https://doi.org/10.22033/ESGF/CMIP6.6113, 2019.

Taylor, P. C., Boeke, R. C., Boisvert, L. N., Feldl, N., Henry, M., Huang, Y., Langen, P. L., Liu, W., Pithan, F., Sejas, S. A., and Tan, I.: Process Drivers, Inter-Model Spread, and the Path Forward: A Review of Amplified Arctic Warming, Frontiers in Earth Science, 9, https://doi.org/10.3389/feart.2021.758361, 2022.

Tebaldi, C. and Arblaster, J. M.: Pattern scaling: Its strengths and limitations, and an update on the latest model simulations, Climatic Change, 122, 459–471, https://doi.org/10.1007/s10584-013-1032-9, 2014.

Tegen, I., Hollrig, P., Chin, M., Fung, I., Jacob, D., and Penner, J.: Contribution of different aerosol species to the global aerosol extinction optical thickness: Estimates from model results, Journal of Geophysical Research: Atmospheres, 102, 23 895–23 915, https://doi.org/10.1029/97jd01864, 1997.

Thuburn, J., Ringler, T., Skamarock, W., and Klemp, J.: Numerical representation of geostrophic modes on arbitrarily structured C-grids, Journal of Computational Physics, 228, 8321–8335, https://doi.org/10.1016/j.jcp.2009.08.006, 2009.

van Marle, M. J. E., Kloster, S., Magi, B. I., Marlon, J. R., Daniau, A.-L., Field, R. D., Arneth, A., Forrest, M., Hantson, S., Kehrwald, N. M., Knorr, W., Lasslop, G., Li, F., Mangeon, S., Yue, C., Kaiser, J. W., and van der Werf, G. R.: Historic global biomass burning emissions for CMIP6 (BB4CMIP) based on merging satellite observations with proxies and fire models (1750–2015), Geoscientific Model Development, 10, 3329–3357, https://doi.org/10.5194/gmd-10-3329-2017, 2017.

van Vuuren, D., O'Neill, B., Tebaldi, C., Chini, L., Friedlingstein, P., Hasegawa, T., Riahi, K., Sanderson, B., Govindasamy, B., Bauer, N., Eyring, V., Fall, C., Frieler, K., Gidden, M., Gohar, L., Jones, A., King, A., Knutti, R., Kriegler, E., Lawrence, P., Lennard, C., Lowe, J., Mathison, C., Mehmood, S., Prado, L., Zhang, Q., Rose, S., Ruane, A., Schleussner, C.-F., Seferian, R., Sillmann, J., Smith, C., Sörensson, A., Panickal, S., Tachiiri, K., Vaughan, N., Vishwanathan, S., Yokohata, T., and Ziehn, T.: The Scenario Model Intercomparison Project for CMIP7 (ScenarioMIP-CMIP7) , https://doi.org/10.5194/egusphere-2024-3765, 2025.

van Vuuren, D. P., Edmonds, J., Kainuma, M., Riahi, K., Thomson, A., Hibbard, K., Hurtt, G. C., Kram, T., Krey, V., Lamarque, J.-F., Masui, T., Meinshausen, M., Nakicenovic, N., Smith, S. J., and Rose, S. K.: The representative concentration pathways: an overview, Climatic Change, 109, 5–31, https://doi.org/10.1007/s10584-011-0148-z, 2011.

Voldoire, A.: CMIP6 simulations of the CNRM-CERFACS based on CNRM-CM6-1 model for CMIP experiment historical, https://doi.org/10.22033/ESGF/CMIP6.4066, 2018.

Voldoire, A.: CNRM-CERFACS CNRM-CM6-1-HR model output prepared for CMIP6 CMIP historical, https://doi.org/10.22033/ESGF/CMIP6.4067, 2019a.

Voldoire, A.: CNRM-CERFACS CNRM-CM6-1-HR model output prepared for CMIP6 ScenarioMIP ssp585, https://doi.org/10.22033/ESGF/CMIP6.4225, 2019b.

Voldoire, A.: CNRM-CERFACS CNRM-CM6-1 model output prepared for CMIP6 ScenarioMIP ssp585, https://doi.org/10.22033/ESGF/CMIP6.4224, 2019c.

Voldoire, A.: CNRM-CERFACS CNRM-ESM2-1 model output prepared for CMIP6 ScenarioMIP ssp585, https://doi.org/10.22033/ESGF/CMIP6.4226, 2019d.

Voldoire, A.: CNRM-CERFACS CNRM-ESM2-1 model output prepared for CMIP6 ScenarioMIP ssp585, https://doi.org/10.22033/ESGF/CMIP6.4226, 2019e.

Volodin, E., Mortikov, E., Gritsun, A., Lykossov, V., Galin, V., Diansky, N., Gusev, A., Kostrykin, S., Iakovlev, N., Shestakova, A., and Emelina, S.: INM INM-CM5-0 model output prepared for CMIP6 CMIP historical, https://doi.org/10.22033/ESGF/CMIP6.5070, 2019a.

Volodin, E., Mortikov, E., Gritsun, A., Lykossov, V., Galin, V., Diansky, N., Gusev, A., Kostrykin, S., Iakovlev, N., Shestakova, A., and Emelina, S.: INM INM-CM5-0 model output prepared for CMIP6 ScenarioMIP ssp585, https://doi.org/10.22033/ESGF/CMIP6.12338, 2019b.

Weijer, W., Cheng, W., Garuba, O. A., Hu, A., and Nadiga, B. T.: CMIP6 Models Predict Significant 21st Century Decline of the Atlantic Meridional Overturning Circulation, Geophysical Research Letters, 47, https://doi.org/10.1029/2019gl086075, 2020.

Wieners, K.-H., Giorgetta, M., Jungclaus, J., Reick, C., Esch, M., Bittner, M., Gayler, V., Haak, H., de Vrese, P., Raddatz, T., Mauritsen, T., von Storch, J.-S., Behrens, J., Brovkin, V., Claussen, M., Crueger, T., Fast, I., Fiedler, S., Hagemann, S., Hohenegger, C., Jahns, T., Kloster, S., Kinne, S., Lasslop, G., Kornblueh, L., Marotzke, J., Matei, D., Meraner, K., Mikolajewicz, U., Modali, K., Müller, W., Nabel, J., Notz, D., Peters-von Gehlen, K., Pincus, R., Pohlmann, H., Pongratz, J., Rast, S., Schmidt, H., Schnur, R., Schulzweida, U.,

https://doi.org/10.5194/egusphere-2026-5525
Preprint. Discussion started: 23 September 2026

Six, K., Stevens, B., Voigt, A., and Roeckner, E.: MPI-M MPI-ESM1.2-LR model output prepared for CMIP6 ScenarioMIP ssp585, https://doi.org/10.22033/ESGF/CMIP6.6705, 2019a.

Wieners, K.-H., Giorgetta, M., Jungclaus, J., Reick, C., Esch, M., Bittner, M., Legutke, S., Schupfner, M., Wachsmann, F., Gayler, V., Haak, H., de Vrese, P., Raddatz, T., Mauritsen, T., von Storch, J.-S., Behrens, J., Brovkin, V., Claussen, M., Crueger, T., Fast, I., Fiedler, S., Hagemann, S., Hohenegger, C., Jahns, T., Kloster, S., Kinne, S., Lasslop, G., Kornblueh, L., Marotzke, J., Matei, D., Meraner, K., Mikolajewicz, U., Modali, K., Müller, W., Nabel, J., Notz, D., Peters-von Gehlen, K., Pincus, R., Pohlmann, H., Pongratz, J., Rast, S., Schmidt, H., Schnur, R., Schulzweida, U., Six, K., Stevens, B., Voigt, A., and Roeckner, E.: MPI-M MPI-ESM1.2-LR model output prepared for CMIP6 CMIP historical, https://doi.org/10.22033/ESGF/CMIP6.6595, 2019b.

Wijngaard, R. R., Herrington, A. R., Lipscomb, W. H., Leguy, G. R., and An, S.-I.: Exploring the ability of the variable-resolution Community Earth System Model to simulate cryospheric–hydrological variables in High Mountain Asia, The Cryosphere, 17, 3803–3828, https://doi.org/10.5194/tc-17-3803-2023, 2023.

Wijngaard, R. R., van de Berg, W. J., van Dalum, C. T., Herrington, A. R., and Levine, X. J.: Arctic temperature and precipitation extremes in present-day and future storyline-based variable resolution Community Earth System Model simulations, Weather and Climate Dynamics, 6, 1241–1266, https://doi.org/10.5194/wcd-6-1241-2025, 2025.

Williams, R. S., Marshall, G. J., Levine, X., Graff, L. S., Handorf, D., Johnston, N. M., Karpechko, A. Y., Orr, A., Van de Berg, W. J., Wijngaard, R. R., and Mooney, P. A.: Future Antarctic Climate: Storylines of Midlatitude Jet Strengthening and Shift Emergent from CMIP6, Journal of Climate, 37, 2157–2178, https://doi.org/10.1175/jcli-d-23-0122.1, 2024.

Wills, R. C. J., Herrington, A. R., Simpson, I. R., and Battisti, D. S.: Resolving Weather Fronts Increases the Large-Scale Circulation Response to Gulf Stream SST Anomalies in Variable-Resolution CESM2 Simulations, Journal of Advances in Modeling Earth Systems, 16, https://doi.org/10.1029/2023ms004123, 2024.

Wu, T., Chu, M., Dong, M., Fang, Y., Jie, W., Li, J., Li, W., Liu, Q., Shi, X., Xin, X., Yan, J., Zhang, F., Zhang, J., Zhang, L., and Zhang, Y.: BCC BCC-CSM2MR model output prepared for CMIP6 CMIP historical, https://doi.org/10.22033/ESGF/CMIP6.2948, 2018.

Xin, X., Wu, T., Shi, X., Zhang, F., Li, J., Chu, M., Liu, Q., Yan, J., Ma, Q., and Wei, M.: BCC BCC-CSM2MR model output prepared for CMIP6 ScenarioMIP ssp585, https://doi.org/10.22033/ESGF/CMIP6.3050, 2019.

Yu, H., Screen, J. A., Xu, M., Hay, S., and Catto, J. L.: Comparing the Atmospheric Responses to Reduced Arctic Sea Ice, a Warmer Ocean, and Increased CO2 and Their Contributions to Projected Change at 2°C Global Warming, Journal of Climate, 37, 6367–6380, https://doi.org/10.1175/jcli-d-24-0104.1, 2024.

Yukimoto, S., Koshiro, T., Kawai, H., Oshima, N., Yoshida, K., Urakawa, S., Tsujino, H., Deushi, M., Tanaka, T., Hosaka, M., Yoshimura, H., Shindo, E., Mizuta, R., Ishii, M., Obata, A., and Adachi, Y.: MRI MRI-ESM2.0 model output prepared for CMIP6 CMIP historical, https://doi.org/10.22033/ESGF/CMIP6.6842, 2019a.

Yukimoto, S., Koshiro, T., Kawai, H., Oshima, N., Yoshida, K., Urakawa, S., Tsujino, H., Deushi, M., Tanaka, T., Hosaka, M., Yoshimura, H., Shindo, E., Mizuta, R., Ishii, M., Obata, A., and Adachi, Y.: MRI MRI-ESM2.0 model output prepared for CMIP6 ScenarioMIP ssp585, https://doi.org/10.22033/ESGF/CMIP6.6929, 2019b.

Zängl, G., Reinert, D., Rípodas, P., and Baldauf, M.: The ICON (ICOsahedral Non-hydrostatic) modelling framework of DWD and MPI-M: Description of the non-hydrostatic dynamical core, Quarterly Journal of the Royal Meteorological Society, 141, 563–579, https://doi.org/10.1002/qj.2378, 2015.

Zappa, G. and Shepherd, T. G.: Storylines of Atmospheric Circulation Change for European Regional Climate Impact Assessment, Journal of Climate, 30, 6561–6577, https://doi.org/10.1175/jcli-d-16-0807.1, 2017.

https://doi.org/10.5194/egusphere-2026-5525
Preprint. Discussion started: 23 September 2026

Ziehn, T., Chamberlain, M., Lenton, A., Law, R., Bodman, R., Dix, M., Wang, Y., Dobrohotoff, P., Srbinovsky, J., Stevens, L., Vohralik, P., Mackallah, C., Sullivan, A., O'Farrell, S., and Druken, K.: CSIRO ACCESS-ESM1.5 model output prepared for CMIP6 ScenarioMIP ssp585, https://doi.org/10.22033/ESGF/CMIP6.4333, 2019a.

Ziehn, T., Chamberlain, M., Lenton, A., Law, R., Bodman, R., Dix, M., Wang, Y., Dobrohotoff, P., Srbinovsky, J., Stevens, L., Vohralik, P., Mackallah, C., Sullivan, A., O'Farrell, S., and Druken, K.: CSIRO ACCESS-ESM1.5 model output prepared for CMIP6 CMIP historical, https://doi.org/10.22033/ESGF/CMIP6.4272, 2019b.